Deficiency in the cell-adhesion molecule *dscaml1* impairs hypothalamic CRH neuron development and neuroendocrine stress axis function

Manxiu Ma[1], Alyssa A. Brunal[1,2], Kareem C. Clark[1], Carleigh Studtmann[1,2], Katelyn Stebbins[1,2,3], Shin-ichi Higashijima[4], Y. Albert Pan[1,5,6]*

1. Fralin Biomedical Research Institute at Virginia Tech Carilion, Virginia Tech, Roanoke, VA 24016, USA

2. Translational Biology Medicine and Health Graduate Program, Virginia Tech, Blacksburg, VA 24061, USA

3. Virginia Tech Carilion School of Medicine, Roanoke, VA 24016, USA

4. National Institutes of Natural Sciences, Exploratory Research Center on Life and Living Systems, National Institute for Basic Biology, Okazaki, Aichi 444-8787, Japan

5. Department of Biomedical Sciences and Pathobiology, Virginia-Maryland College of Veterinary Medicine, Virginia Tech, Blacksburg, VA 24060, USA

6. Department of Psychiatry and Behavioral Medicine, Virginia Tech Carilion School of Medicine, Roanoke, VA 24016, USA

*Correspondence should be addressed to Y. Albert Pan, email: yapan@vtc.vt.edu

ABSTRACT

The corticotropin-releasing hormone (CRH)-expressing neurons in the hypothalamus are critical regulators of the neuroendocrine stress response pathway, known as the hypothalamic-pituitary-adrenal (HPA) axis. As developmental vulnerabilities of CRH neurons contribute to stress dysfunction and mental health disorders, it is critical to identify the molecular mechanisms underlying normal and abnormal CRH neuron development. Using zebrafish, we identified *Down syndrome cell adhesion molecule like-1* (*dscaml1*) as an integral mediator of CRH-neuron development and stress axis function. In *dscaml1* mutant animals, CRH neurons had higher stress axis-associated neuropeptide (*crhb* and *avp*) expression, increased cell number, decreased apoptosis, and reduced intercellular spacing as compared to controls. Time-lapse imaging showed that CRH neuron cell death is reduced in *dscaml1* mutant animals, contributing to increased CRH neuron number. Physiologically, *dscaml1* mutant animals had significantly higher baseline stress hormone (cortisol) levels and an attenuated response to acute stressors. Together, these findings identify *dscaml1* as an essential factor for stress axis development and suggest that stress axis dysregulation may contribute to the etiology of human *DSCAML1*-linked neuropsychiatric disorders.

INTRODUCTION

The hypothalamic corticotropin-releasing hormone (CRH)-expressing neurons are the central regulators of the neuroendocrine stress response pathway, known as the hypothalamic-pituitary-adrenal (HPA) axis in mammals or the hypothalamic-pituitary-interrenal (HPI) axis in fish (Denver, 2009). Upon exposure to environmental disturbances (i.e., stressors), stress-related neural inputs converge on hypothalamic CRH neurons to activate a hormonal cascade that ultimately leads to the release of glucocorticoids, which

44 have broad effects on cognitive, affective, and immune functions (Spencer and Deak, 2017;
45 McEwen and Akil, 2020).

46 The development of CRH neurons profoundly affects the function of the HPA and HPI axis
47 (collectively referred to as the stress axis). Developmental perturbations of CRH neurons,
48 particularly in early-life periods, lead to long-term changes in CRH neuron function (Regev
49 and Baram, 2014). Additionally, rodent models demonstrate that dysregulation of CRH
50 neurons increases anxiety- and depressive-like phenotypes (Keen-Rhinehart et al., 2009;
51 Kolber et al., 2010). Elevated CRH expression in the corticospinal fluid and hypothalamus
52 has also been found in human depression (Nemeroff et al., 1984; Raadsheer et al., 1995;
53 Merali et al., 2006). These preclinical and clinical studies underscore the need to identify the
54 genes and molecules mediating CRH-neuron development and determine how
55 developmental perturbations affect HPA-axis function.

56 Previous studies in animal models have elucidated how hypothalamic CRH neurons are
57 generated from progenitors in the ventral diencephalon (Alvarez-Bolado, 2019; Nagpal et al.,
58 2019; Placzek et al., 2020). Secreted factors including FGF10, SHH, BMPs, and Nodal first
59 define the anterior-dorsal hypothalamic domain; within this domain, CRH neurons are
60 progressively specified by a combination of key transcription factors, including Fezf2, Otp,
61 Sim1, Arnt2, and Brn2. Once specified, CRH neurons need further differentiation, such as
62 neuronal morphogenesis, synaptogenesis, epigenetic programming, and cell death, to
63 establish a functional stress-responsive neural circuit. These later stages of neuronal
64 differentiation are shaped by intercellular interactions, which are mediated by membrane-
65 localized cell-adhesion molecules (Moreland and Poulain, 2022). The specific cell-adhesion
66 molecules that mediate developmental signaling in CRH neurons are still unknown.

67 To address this knowledge gap, we utilized zebrafish (*Danio rerio*) as the model. The
68 structure and function of the mammalian HPA axis and the teleostean HPI axis are highly
69 conserved (Wendelaar Bonga, 1997; Lohr and Hammerschmidt, 2011). In mammals, the CRH
70 neurons that are involved in HPA-axis activation are in the hypothalamic paraventricular
71 nucleus (PVN). In teleosts (ray-finned fish), the neuroendocrine preoptic area (NPO) is
72 ontogenically equivalent to the PVN, and CRH neurons within the NPO perform the same role
73 as their mammalian counterparts (Herget and Ryu, 2015). A unique advantage of the
74 zebrafish system is its rapid and external development. The development of the HPI axis
75 begins between 1-2 days post fertilization (dpf), and stress-induced cortisol signaling and
76 behaviors can be observed at 4-5 dpf (Alsop and Vijayan, 2008; Alderman and Bernier, 2009;
77 Bai et al., 2016). The rapid development and translucency of zebrafish allow direct
78 microscopic observation of CRH neuron development in intact, developing animals.
79 In this study, we investigated the contributions of a conserved neuronal signaling
80 molecule—*Down syndrome cell adhesion molecule-like 1* (zebrafish gene: *dscaml1;* mouse
81 gene: *Dscaml1;* Human gene: *DSCAML1*; Protein: DSCAML1). DSCAML1 is one of two DSCAM
82 family members in vertebrates, the other being DSCAM (Garrett et al., 2012). Unlike
83 invertebrate DSCAMs, vertebrate DSCAMs are not significantly alternatively spliced (Sanes
84 and Zipursky, 2020). In the mammalian retina, DSCAML1 prevents excessive aggregation
85 between cells of the same type (homotypic aggregation) and promotes developmental cell
86 death (Fuerst et al., 2009; Garrett et al., 2016). DSCAML1 also acts to refine synaptic
87 specificity and synapse number (Yamagata and Sanes, 2008; Sachse et al., 2019). In humans,
88 rare variants in *DSCAML1* are associated with several neurodevelopmental disorders,
89 including autism spectrum disorder, cortical abnormality, and epilepsy (Iossifov et al., 2014;

90 Karaca et al., 2015; Hayase et al., 2020; Ogata et al., 2021). Genetic and epigenetic studies
91 also implicate *DSCAML1* in the stress response to violent experiences (Caramillo et al., 2015;
92 Saadatmand et al., 2021). However, the relationship between *DSCAML1* and the stress axis
93 remains unknown.

94 Using zebrafish, we previously explored how DSCAML1 affects neural pathways and
95 systemic functions (Ma et al., 2020a; Ma et al., 2020b). We found that *dscaml1* deficiency
96 resulted in various physiological and behavioral deficits, including darker pigmentation,
97 slower light adaptation, and slower eye movements (saccades) (Ma et al., 2020b).
98 Interestingly, darker pigmentation and slower light adaptation can also be caused by
99 abnormal glucocorticoid receptor signaling, as seen in the zebrafish *glucocorticoid receptor*
100 (*gr*) mutants, raising the possibility that the HPI-axis may be dysfunctional in *dscaml1*
101 mutants (Griffiths et al., 2012; Muto et al., 2013).

102 In the present study, we report that *dscaml1* deficiency in zebrafish perturbs CRH neuron
103 development and hyperactivates the HPI axis. These findings show that DSCAML1 is
104 necessary for normal stress axis development and raise the possibility that stress
105 dysfunction contributes to human *DSCAML1*-linked disorders.

106 RESULTS

107 *dscaml1* deficiency results in overexpression of neuroendocrine factors

108 To gain an unbiased view of the molecular changes resulting from *dscaml1* deficiency, we
109 compared the transcriptomic profiles between *dscaml1* homozygous mutant (*dscaml1*-/-)
110 and control (wild type) animals using RNA sequencing (RNA-seq). cDNA from whole 3.5-4
111 days post-fertilization (dpf) *dscaml1*-/- and control larvae were sequenced using an Illumina

112 next-generation sequencer. Using a threshold of at least two-fold change and an adjusted *p*-
113 value of less than 0.01, we identified 25 upregulated and 79 downregulated genes (Fig. 1A,
114 Supplementary file 1).

115 Among the 25 upregulated genes in the *dscaml1*-/- animals, 7 were secreted
116 neuropeptides/hormones expressed in the hypothalamus or pituitary: *corticotropin-*
117 *releasing hormone b (crhb)*, *parathyroid hormone 2* (*pth2*), *somatolactin beta (smtlb), cocaine-*
118 *and amphetamine-regulated transcript 3 (cart3), proopiomelanocortin a (pomca), arginine*
119 *vasopressin (avp),* and *spexin hormone (spx).* Among them, three (*crhb, avp, pomca)* are core
120 regulators of the HPI axis (Alsop and Vijayan, 2009; Lohr and Hammerschmidt, 2011). *crhb*
121 encodes the zebrafish CRH; *avp* encodes the neuropeptide AVP that controls osmolarity,
122 blood pressure, and synergizes with CRH to promote cortisol release; *pomca* encodes the
123 adrenocorticotropic hormone (ACTH), the primary pituitary hormone that triggers
124 glucocorticoid release. Additionally, two genes involved in apoptosis are upregulated: *BCL2*
125 *apoptosis regulator b* (*bcl2b)* and *phorbol-12-myristate-13-acetate-induced protein 1*
126 *(pmaip1/noxa)*. Protein class categorization analysis with PANTHER revealed intercellular
127 signal molecule as the largest class (4 genes, 16%) (Fig. 1B) (Mi et al., 2021).

128 The 79 genes downregulated in the *dscaml1*-/- animals are more diverse in function
129 compared to the upregulated genes. Protein class categorization analysis with PANTHER
130 identified the largest protein classes as metabolite interconversion enzymes (12 genes,
131 15.19%), protein-binding activity modulators (9 genes, 11.39%), transporters (8 genes,
132 10.13%), and defense/immunity protein (6 genes, 7.59%) (Fig. 1C). We noted that 30 of the
133 79 (38%) downregulated genes are highly expressed in the liver, and 10 of these genes are
134 involved in innate immunity and the complement cascade (Fig. 1A, Supplementary file 2).

135 These results suggest that liver function and innate immunity may be suppressed in the
136 *dscaml1* mutants.

137 To identify the signaling pathways affected by *dscaml1* deficiency, we analyzed all
138 differentially expressed genes (*p<0.01*, 210 mapped genes) using the statistical enrichment
139 test (PANTHER Classification System, version 17.0) (Mi et al., 2021). All significantly
140 enriched (FDR<*0.05*) Gene Ontogeny (GO) terms for molecular function relate to the parent
141 GO term *hormone activity* (Fig. 1D). The PANTHER pathway analysis also identified another
142 significant stress modulating neuropeptide, *adenylate cyclase activating polypeptide 1b*
143 (*adcyap1b*, also known as *PACAP*) that is significantly upregulated (0.66 fold change,
144 adjusted *p<0.0001*) (Stroth et al., 2011).

145 Together, our transcriptomic analyses indicate that *dscaml1* deficiency results in the
146 upregulation of neuropeptide/hormonal signaling and the downregulation of liver and
147 innate immune function. Suppression of liver and immune function is a hallmark of stress
148 axis activation, which is consistent with the overexpression of the principal neuropeptides
149 involved in the stress axis: *crhb, avp*, *pomca,* and *adcyap1b*.

150 ***dscaml1* deficiency alters the development of CRH neurons in the NPO**

151 Considering the RNA-seq findings, we tested whether *dscaml1* deficiency perturbs the
152 development of the CRH neurons in the NPO—the central regulators of the stress axis in
153 teleosts (Nagpal et al., 2019). Compared to mammalian CRH neurons in the PVN, CRH
154 neurons in the zebrafish NPO (henceforth referred to as CRH^{NPO} neurons) are more
155 homogenous in their neurotransmitter usage (Romanov et al., 2017; Short et al., 2021).
156 Nearly all (>95%) CRH^{NPO} neurons are glutamatergic, and they predominantly co-express
157 *avp* (Herget and Ryu, 2015; Lovett-Barron et al., 2020). Double fluorescent *in situ*

158 hybridization (FISH) with antisense riboprobes against *crhb* and *avp* show found that most
159 *crhb+* neurons are *avp+* (82.85±6.01%), and all *avp+* neurons are *crhb*+ (100±0.00%) (Fig.
160 2A-D). Therefore, *avp*-expressing neurons are a major subset of CRH^{NPO} neurons (referred to
161 as $CRH^{NPO\text{-}AVP}$ neurons from here on).

162 To examine the developmental trajectory of CRH^{NPO} (*crhb+*) and $CRH^{NPO\text{-}AVP}$ (*avp+*)
163 neurons, we focused on three developmental stages: 2, 3, and 5 dpf. These stages span the
164 period between the birth of these neurons (~1 dpf) and the onset of stress axis responsivity
165 (4-5 dpf) (Alderman and Bernier, 2009; Clark et al., 2011). We found that *dscaml1* is
166 expressed in CRH^{NPO} neurons during this period (Supplementary Fig. 1). Using single FISH
167 for *crhb* and *avp*, we quantified the number of cells in each cell group and the relative
168 expression of *crhb* and *avp* (using the median FISH signal intensity per cell, see methods).

169 Additionally, given that DSCAML1 prevents homotypic cellular aggregation in the retina
170 (Fuerst et al., 2009; Ma et al., 2020b), we tested whether CRH neurons become aggregated
171 in *dscaml1* mutants. We measured homotypic aggregation by counting the number of close
172 cellular contacts between cells of the same subtype (CRH^{NPO} or $CRH^{NPO\text{-}AVP}$ neurons) (Ma et
173 al., 2020b). More close contacts indicate a higher degree of homotypic cellular aggregation.
174 As the average cell diameter is around 10 μm, cells are deemed to be in close contact when
175 the centers of the cells are within 10 μm.

176 For CRH^{NPO} neurons, *dscaml1* deficiency increased cell number and *crhb* expression, but
177 cellular aggregation was unaffected (Fig. 2E-I). The number of CRH^{NPO} neurons progressively
178 increased over time, from 14.78 cells (2 dpf) to 18.85 cells (3 dpf) to 26.60 cells (5 dpf) per
179 animal in WT (Fig 2E-E″, G). In *dscaml1*-/- animals, the number of CRH^{NPO} neurons increased
180 at a higher rate, from 12.67 cells (2 dpf) to 19.46 cells (3 dpf) to 36.39 cells (5 dpf) per animal

181 (Fig. 2F-F″, G). We found a significant difference in cell number by developmental stage and
182 genotype, and there was a significant interaction between stage and genotype (Two-way
183 ANOVA, Supplementary Table I). Pair-wise comparisons with Holm-Sidak correction found
184 a significant increase in cell number between *dscaml1-/-* and WT animals at 5 dpf but not at
185 2 and 3 dpf (Fig 2G, adjusted *p* values as shown).

186 The level of *crhb* expression (median FISH intensity level among *crhb+* neurons in each
187 sample) was increased in *dscaml1-/-* animals. We found a significant difference in signal
188 intensity per cell by developmental stage and genotype, and there was a significant
189 interaction between stage and genotype (two-way ANOVA, Supplementary Table I). Pair-
190 wise comparisons with Holm-Sidak correction found a significant increase at 3 and 5 dpf but
191 not at 2 dpf (Fig 2H). In contrast, we did not observe any significant differences in the number
192 of contacts per cell, either overall or at specific developmental stages (Fig. 2I).

193 For $CRH^{NPO\text{-}AVP}$ neurons (*avp+*), *dscaml1* deficiency also increased cell number and *avp*
194 signal intensity per cell. In contrast to CRH^{NPO} neurons, *dscaml1* deficiency resulted in
195 significant aggregation between $CRH^{NPO\text{-}AVP}$ neurons (Fig. 3). The number of $CRH^{NPO\text{-}AVP}$
196 neurons progressively increased over time, increasing from 9.89 cells (2 dpf) to 17.33 cells
197 (3 dpf) to 20.93 cells (5 dpf) per animal in WT (Fig. 3A-A″, C). In *dscaml1-/-* animals, the
198 number of $CRH^{NPO\text{-}AVP}$ neurons increased at a higher rate, from 14.11 cells (2 dpf) to 19.33
199 cells (3 dpf) to 34.00 cells (5 dpf) per animal (Fig. 3B-B″, C). We found a significant difference
200 in cell number by developmental stage and genotype, and there was a significant interaction
201 between stage and genotype (two-way ANOVA, Supplementary Table I). Pair-wise
202 comparisons with Holm-Sidak correction found a significant increase at 5 dpf but not at 2
203 and 3 dpf (Fig 3C, adjusted *p* values as indicated). Outside of the NPO, we also observed

204 apparent increases in cell number and *crhb* signal intensity at 5 dpf, suggesting that extra-
205 hypothalamic CRH neuron populations are likely also impacted by *dscaml1* deficiency (Fig.
206 2E″, F″)

207 The level of *avp* expression was increased in *dscaml1*-/- animals. We found a significant
208 difference in *avp* FISH signal intensity by developmental stage and genotype, and there was
209 a significant interaction between stage and genotype (two-way ANOVA, Supplementary
210 Table I). Pair-wise comparisons with Holm-Sidak correction found a significant increase at 3
211 dpf but not at 2 and 5 dpf (Fig. 3D, adjusted *p* values as indicated). For the number of contacts
212 per cell, we found a significant difference in FISH signal intensity by developmental stage
213 and genotype, and there was a significant interaction between stage and genotype
214 (Supplementary Table I). Pair-wise comparisons with Holm-Sidak correction found a
215 significant increase at 5 dpf but not at 2 and 3 dpf (Fig 3E, adjusted *p* values as indicated).

216 Overall, the effects of *dscaml1* deficiency on CRH neurons become more pronounced as
217 the animals progress developmentally. There were no significant differences at 2 dpf, when
218 the stress axis is not yet responsive. However, at 3 and 5 dpf, we observed significant
219 increases in cell number and *crhb*/*avp* expression. Cellular aggregation, as measured by the
220 amount of close cellular contact, was significantly increased only within the $CRH^{NPO\text{-}AVP}$
221 subgroup (Fig. 3E). There is, however, a mild (and non-significant) increase in close cellular
222 contact in the broader CRH^{NPO} population. The stronger effect on the more defined $CRH^{NPO\text{-}}$
223 ^{AVP} population is consistent with the idea that *dscaml1* acts homotypically to prevent
224 aggregation and that CRH^{NPO} neurons contain multiple subtypes.

225 **Impairments of CRH^{NPO} neurons in *dscaml1* mutants are independent of ambient light**

226 Our previous study showed that *dscaml1* mutants likely have impaired ambient light
227 perception (Ma et al., 2020b). As ambient light is a major driver of baseline stress axis activity
228 (Spencer and Deak, 2017), we examined whether *dscaml1* deficiency affects CRH^{NPO} and
229 $CRH^{NPO\text{-}AVP}$ neuron development in the absence of light. Experimental animals were reared
230 in constant darkness from 4 hours post-fertilization (hpf) (sphere stage)(Kimmel et al., 1995)
231 until they were anesthetized and fixed at 3 or 5 dpf. FISH with *crhb* and *avp* probes were
232 performed to identify CRH^{NPO} and $CRH^{NPO\text{-}AVP}$ neurons, respectively.

233 For CRH^{NPO} neurons, we observed similar effects of *dscaml1* deficiency in dark-reared
234 animals compared to those under normal light-dark cycles (Fig. 4A-C). Comparing dark-
235 reared WT and *dscaml1-/-* animals, we found a significant difference in cell number by
236 developmental stage and genotype (two-way ANOVA, Supplementary Table I). There was no
237 significant interaction between stage and genotype, indicating that both stages are similarly
238 affected by *dscaml1* deficiency. For *crhb* FISH signal intensity and the number of contacts per
239 cell, there was a significant difference by genotype but no significant difference by stage or
240 interaction. We found significant increases in all pair-wise comparisons between WT vs.
241 *dscaml1*-/- groups, except for the number of cell contacts at 5 dpf (Fig 4A-C, Holm-Sidak
242 correction adjusted *p* values as indicated).

243 For $CRH^{NPO\text{-}AVP}$ neurons, we also observed similar effects of *dscaml1* deficiency in dark-
244 reared animals compared to those under normal light-dark cycles (Fig. 4D-F). Comparing
245 dark-reared WT and *dscaml1-/-* animals, we found a significant difference in cell number and
246 *avp* FISH signal intensity by developmental stage and genotype (two-way ANOVA,
247 Supplementary Table I). There was no significant interaction between stage and genotype,
248 indicating that both stages are affected by *dscaml1* deficiency similarly. For the number of

249 contacts per cell, there was a significant difference by genotype but no significant difference
250 by stage or interaction. We found significant increases in all pair-wise comparisons between
251 WT vs. *dscaml1*-/- groups (Fig. 4D-F, Holm-Sidak correction adjusted *p* values as indicated).
252 Overall, we observed consistent developmental phenotypes in CRH^{NPO} and $CRH^{NPO\text{-}AVP}$
253 neurons under both normal light-dark cycles and constant darkness. These results suggest
254 that the deficit in ambient light detection is not a key contributor to the developmental
255 changes in NPO neurons caused by *dscaml1* deficiency.

256 **CRH neuron cell death depends on *dscaml1***

257 The increase in CRH^{NPO} neuron number and aggregation of cells of the same subtype are
258 reminiscent of mouse mutants deficient in programmed cell death (PCD)(Keeley et al., 2012;
259 Chen et al., 2013). Mouse *Dscaml1* mutants also exhibited a notable reduction in neuronal
260 cell death in the retina (Garrett et al., 2016). Therefore, we reasoned that *dscaml1* deficiency
261 might increase CRH^{NPO} neuron number by impairing PCD.
262 To test this, we first used an anti-activated-caspase 3 (AC3) antibody to label apoptotic
263 cells. Consistent with previous findings, we found widespread apoptosis in the nervous
264 system in wild-type animals, peaking at 3 dpf (Supplementary Fig. 2A-A″)(Cole and Ross,
265 2001). In *dscaml1-/-* animals, there is a decrease in AC3-positive cells at 3 and 5 dpf,
266 compared to wild-type controls (Supplementary Fig. 2B-B″). Using the Z-Brain region-
267 specific quantification method (Randlett et al., 2015), we found that *dscaml1* deficiency
268 significantly reduced cell death in the forebrain and midbrain, including the NPO
269 (Supplementary Fig. 2C-D). This result shows that *dscaml1* is necessary to promote PCD in
270 the brain during development.

271 To further determine whether *dscaml1* affects the survival of CRH^{NPO} neurons, we tracked
272 the fate of individual CRH neurons during the peak of PCD (3-5 dpf) using *in vivo* time-lapse
273 imaging. To visualize CRH^{NPO} neurons in live zebrafish, we generated a *crhb* knock-in
274 fluorescent reporter line using CRISPR-mediated genomic insertion (Fig. 5A) (Kimura et al.,
275 2014). A Cre-switchable *hsp-LoxP-RFP-LoxP-GFP* cassette was inserted 35 base pairs
276 upstream of the first exon of *crhb* so that the expression of RFP (without Cre-mediate
277 recombination) or GFP (with Cre-mediate recombination) would mark the endogenous *crhb*-
278 expressing cells (Fig. 5B).

279 The resulting transgenic line, *crhb:LoxP-RFP-LoxP-GFP* (*crhb:LRLG*), has RFP and GFP
280 expression pattern that matches the endogenous *crhb* transcript expression patterns (Fig.
281 5C-D, compare to Fig. 2E″). To validate the fidelity of fluorescent reporter gene expression,
282 we examined whether *crhb:LRLG*-labeled cells in the NPO express CRH protein. In animals
283 not exposed to Cre (default RFP expression), we found that most RFP+ (84.71±2.19%)
284 neurons are CRH immunopositive (Supplementary Fig. 3A-B). Together, these results
285 indicate that the *crhb:LRLG* line reliably labels CRH^{NPO} neurons.

286 For *crhb:LRLG*-labeled CRH^{NPO} neurons, *dscaml1* deficiency also increased the number of
287 cells (Fig. 5E-F). We found significant differences by age and genotype, with no significant
288 interaction between the two (two-way ANOVA, Supplementary Table I). There was a
289 significantly higher number of RFP-positive neurons in the *dscaml1* mutants at 5 dpf (n=16
290 for WT and 17 for *dscaml1-/-*) but not 3 dpf (n=5 for WT and 11 for *dscaml1-/-*) (Fig. 5G,
291 multiple comparison test with Holm-Sidak correction). This result corroborates our *crhb*
292 FISH results that show increased CRH^{NPO} neuron number in *dscaml1* mutants (Fig. 2G).

293 Using the *crhb:LRLG* line, we performed time-lapse imaging in anesthetized animals. We
294 induced partial Cre-mediated recombination by injecting *CreER* mRNA at the 1-cell stage and
295 adding 4-hydroxytamoxifen (4-OHT) to activate CreER at 6-24 hpf (Fig. 5B). At 3-4 dpf,
296 intermingled GFP+ and RFP+ cells can be seen in the NPO by confocal imaging (Fig. 5H-H″
297 and Supplementary video 1). Over time, some cells appear to travel away from the CRH^{NPO}
298 neuron cluster. We reasoned that these cells were apoptotic cells carried away by microglia,
299 as seen in previous zebrafish studies (Mazaheri et al., 2014). To confirm this, we induced GFP
300 expression (by full Cre-mediated recombination) in all *crhb:LRLG*-labeled cells and labeled
301 microglia with mCherry, a red fluorescent protein (Fig. 5I-I″ and Supplementary video 2)
302 (Espenschied et al., 2019). Indeed, mCherry+ microglia migrated toward the GFP+ cell
303 cluster, engulfed GFP-positive cells, and carried the presumably apoptotic cells away. The
304 remnant of the engulfed cell can be seen inside a large vacuole within the microglia (Fig. 5J-
305 J′). These results suggest that CRH^{NPO} neurons undergo PCD and that dying cells are rapidly
306 removed by microglia.
307 To track the fate of individual CRH^{NPO} neurons, we performed two-photon imaging from
308 3 to 5 dpf. To minimize the potential effects of stress on PCD (Irles et al., 2014), we
309 anesthetized and immobilized the animals during imaging (Fig. 6A). In between imaging
310 sessions, each animal is allowed to recover in individual wells of 12-well plates, under
311 normal light-dark cycles. Cells that are present at the first time point (78 hpf) were tracked
312 at four subsequent time points (84, 96, 108, and 120 hpf) and categorized as either persisting
313 (present at the last time point) or lost (lost at any of the following time points) (Fig. 6B-B″).
314 Overall, we observe a trend of reduced cell loss in the *dscaml1*+/- and *dscaml1-/-* animals
315 (Chi-square test for trend, p=0.0398) (Fig. 6C, total number of tracked cells as indicated). In

316 WT animals, 16.41% of cells are lost, versus 10.91% and 7.53% for *dscaml1*+/- *and dscaml1*-
317 /-, respectively. The difference in the rate of cell loss (8.9%) accounts for a significant portion
318 (but not all) of the difference in CRH^{NPO} neuron cell number.

319 Finally, considering the timing of cell loss, we plotted the survival curve of CRH^{NPO}
320 neurons for each genotype. Again, there was a significant difference in the trends of cell loss
321 (Logrank test for trend, p=0.0098), with the *dscaml1*-/- animals consistently showing a
322 higher survival rate (Fig. 6D). Together, these results show that *dscaml1* deficiency reduces
323 PCD of CRH^{NPO} neurons, which potentially contribute to the hyperactivation of the stress axis.

324 **Baseline and stress-induced cortisol levels are elevated in *dscaml1* mutant animals**

325 Given the developmental perturbation of CRH^{NPO} neurons and the global changes and
326 gene expression, we next determined whether the hormonal output of the stress axis is
327 altered. We examined the level of cortisol, the primary stress hormone in zebrafish and
328 humans. Cortisol levels were measured using an enzyme-linked immunosorbent assay
329 (ELISA) on homogenates made from pools of 5 dpf animals (30 animals per sample, 6
330 samples per condition). All animals were raised at the same density with a normal circadian
331 cycle (14 h day/10 h night). Under this circadian cycle, *dscaml1* mutant animals exhibit
332 similar diurnal locomotor rhythm as wild-type animals (Ma et al., 2020b).

333 Multiple baseline and stressed conditions were tested to evaluate potential alterations of
334 cortisol in the control and mutant animals. To measure baseline cortisol, we collected
335 animals within 30 min after light onset (zeitgeber time 0, ZT0) and in the afternoon (ZT6-8).
336 For stress-induced cortisol measurements, acute stressors were applied at ZT6-8. We
337 exposed 5 dpf animals to stirring stress (swirling water, 5 minutes)(Castillo-Ramirez et al.,
338 2019) or hyperosmotic stress (250 mM NaCl, 20 minutes) at ZT6-8 (Yeh et al., 2013). These

339 are well-characterized acute stressors comparable to the water current and salinity changes
340 experienced by zebrafish larvae in their natural habitat.

341 Overall, *dscaml1-/-* animals exhibited higher levels of cortisol than control animals across
342 all conditions (Multiple Mann-Whitney test with Holm-Sidak correction. Adjusted *p* values
343 shown in Fig. 7A). At ZT0, the *dscaml1* mutant baseline cortisol levels were 2.7-fold higher
344 than that of controls (median 350.06 pg/ml versus 129.80 pg/ml). The difference in cortisol
345 was less pronounced at ZT6-8, but *dscaml1* mutants still had significantly higher cortisol
346 levels than controls at baseline and after acute stress.

347 In addition to elevated baseline cortisol levels, *dscaml1* mutant animals exhibited
348 attenuated cortisol induction by acute stressors. In the control group, stirring stress and
349 hyperosmotic stress produced an 88% and 95% increase in cortisol over the ZT6-8 baseline,
350 respectively. The response to hyperosmotic stress was more robust (p=0.016) than that
351 generated by stirring stress (p=0.0798, Kruskal-Wallis test with Dunn's correction). In the
352 *dscaml1-/-* group, stirring stress and hyperosmotic stress only produced 29% and 49%
353 increases in cortisol over the ZT6-8 baseline, respectively. These increases were not
354 statistically significant (p=0.811 for stirring stress, p=0.1364 for hyperosmotic stress).
355 Together, these results show that *dscaml1* deficiency increases the baseline activity of the
356 neuroendocrine stress axis, which potentially contributes to less robust stress-induced
357 cortisol production.

358 ***dscaml1* mutants are responsive to glucocorticoids**

359 As mentioned earlier, we found visual response deficiencies in *dscaml1* mutants that
360 resembled zebrafish with deficient *glucocorticoid receptor (gr)* signaling (Griffiths et al.,
361 2012; Muto et al., 2013; Ziv et al., 2013). Like *dscaml1-/-* animals, the *gr* mutants also

362 exhibited elevated baseline cortisol and overexpression of *crhb* (Ziv et al., 2013). These
363 findings suggest that *dscaml1* deficiency may result from insufficient glucocorticoid
364 receptor-mediated signaling. To test this, we examined whether *dscaml1* mutants can
365 respond transcriptionally to exogenously applied glucocorticoids. We examined the
366 expression of *crhb* and *avp* in the NPO, as these neuropeptides are under feedback control
367 from glucocorticoid-glucocorticoid receptor signaling (Watts, 2005).

368 A synthetic glucocorticoid receptor agonist, dexamethasone (Dex), was added to the
369 embryo media at a final concentration of 2 μM from 4 to 5 dpf (24 hours). Vehicle (0.02%
370 ethanol) treated siblings were used for comparison. For *crhb* transcript level in CRH^{NPO}
371 neurons, we found significant differences caused by Dex treatment and genotype, with
372 significant interaction between the two (two-way ANOVA, Supplementary Table I). Multiple
373 comparison tests found that Dex significantly reduced *crhb* transcript level in *dscaml1-/-*
374 animals but not in wild-type animals (Holm-Sidak correction, Fig. 7B with *p* values as
375 indicated). For *avp* transcript level in $CRH^{NPO\text{-}AVP}$ neurons, we found significant differences
376 caused by Dex treatment and genotype, with no significant interaction (two-way ANOVA,
377 Supplementary Table I). Multiple comparison tests found that Dex significantly increases *avp*
378 transcript level in *dscaml1-/-* animals but not in wild-type animals (Holm-Sidak correction,
379 Fig. 7C). Together, these results show that *dscaml1* deficiency does not result in a loss of
380 glucocorticoid responsivity in CRH^{NPO} and $CRH^{NPO\text{-}AVP}$ neurons. Instead, *dscaml1-/-* animals
381 are more susceptible to changes in glucocorticoid levels than wild-type siblings, which may
382 exacerbate stress axis dysfunction in the *dscaml1-/-* animals.

383 **DISCUSSION**

384 In summary, the present study provides evidence that *dscaml1* regulates the
385 development and number of hypothalamic CRH neurons, a crucial component of the
386 vertebrate neuroendocrine stress axis. In zebrafish *dscaml1* mutants, hypothalamic CRH
387 neurons (CRH^{NPO} neurons) have increased stress axis-associated neuropeptide expression,
388 increased cell number, decreased programmed cell death, and reduced cellular spacing. We
389 show that *dscaml1* mutants have reduced CRH^{NPO} neuron cell death, resulting in a higher
390 number of CRH neurons. These developmental deficits likely contribute to the stress axis
391 dysfunction seen in *dscaml1* mutant animals, including elevated cortisol levels at baseline
392 and attenuated cortisol induction after acute stress (Fig. 7D). Together, these findings
393 strongly link DSCAML1 to the development of the stress axis and shed new light on the
394 potential etiology of human *DSCAML1*-linked mental health conditions.

395 **DSCAML1 is a novel intercellular signaling molecule for CRH neuron development**

396 To our knowledge, DSCAML1 is the first intercellular signaling molecule to be implicated
397 in normal CRH neuron development. As such, further understanding of DSCAML1 will help
398 bridge the knowledge gap on the differentiation events after the onset of transcriptional cell
399 fate specification and provide insights on what naturally occurring maturation processes
400 may be perturbed by clinically relevant early-life stressors (Chen and Baram, 2016; van
401 Bodegom et al., 2017).

402 DSCAML1 has been most extensively studied in the vertebrate retina, a structure with
403 precise laminar organization and cells that are evenly distributed in the planar plane. In
404 contrast, the hypothalamic CRH neurons are located in a non-laminated brain area where
405 neurons of the same subtype are often clustered. Further investigation of DSCAML1 in the

406 hypothalamus will provide insights into the shared and unique intercellular signaling
407 mechanisms between laminar and non-laminar brain organization.

408 **Mechanism of stress axis hyperactivation in DSCAML1 deficient animals**

409 The *dscaml1*-/- animals exhibit multiple signs of stress axis hyperactivation, including
410 cortisol elevation and the suppression of immunity-associated genes. One potential cause of
411 these phenotypes may be the overexpression of *crhb* and *avp* in the hypothalamus. In mice,
412 broad overexpression of CRH leads to elevated corticosterone (the stress glucocorticoid in
413 rodents) and produces phenotypes similar to Cushing's syndrome, a human disorder caused
414 by the overproduction of cortisol (Stenzel-Poore et al., 1992; Arnett et al., 2016). The
415 potential effects of chronically elevated AVP are less understood, but increased AVP
416 signaling likely potentiates stress axis activity (René et al., 2002).

417 Beyond dysfunction of hypothalamic neurons, a broader neurological imbalance can also
418 activate the stress axis. Seizures have been shown to activate the stress axis, which increases
419 the likelihood of future seizures (O'Toole et al., 2014; Hooper et al., 2018). It has been
420 reported that *Dscaml1* mutant rats and human patients with *DSCAML1* loss-of-function
421 variants exhibit neuronal hyperactivation and seizures. It is, therefore, possible that
422 excitation-inhibition imbalance in extra-hypothalamic regions may result in increased
423 CRH^{NPO} neuron firing in zebrafish *dscaml1* mutants. Further studies on the cell-type specific
424 functions of *dscaml1* are needed to understand the precise cause of stress axis
425 hyperactivation in *dscaml1*-/- animals.

426 **DSCAML1-mediated regulation of CRH neuron cell number**

427 During development, PCD is critical for eliminating transient cell types, matching input
428 and output cell populations, and maintaining cellular spacing (Yamaguchi and Miura, 2015;
429 Wong and Marin, 2019). It has been hypothesized that PCD in the hypothalamus may specify
430 neural circuit assembly and shape output activity (Simerly, 2002; Forger, 2009). Congruent
431 with this idea, reduced hypothalamic PCD caused by early-life stress is associated with
432 increased sensitivity to acute stressors in adulthood (Zhang et al., 2012; Irles et al., 2014).
433 As an intercellular signaling molecule, DSCAML1 may act to transduce extracellular cell
434 death cues. One possible extracellular cue for CRH neuron cell death is homotypic
435 intercellular contact, which triggers the process known as proximity-based cell death (Chen
436 et al., 2013). In proximity-based cell death, a cell immediately adjacent to another cell of the
437 same type is more likely to undergo PCD. In the retina, this process helps establish even tiling
438 of different cell types across the visual field. However, the role of proximity-based cell death
439 outside of the retina is still unclear. In *dscaml1*-/- animals, we found increased homotypic
440 contacts between the $CRH^{NPO\text{-}AVP}$ neurons. It is possible that the additional homotypic
441 contacts are from $CRH^{NPO\text{-}AVP}$ neurons that had failed to undergo proximity-based cell death
442 due to *dscaml1* deficiency. Further work is needed to determine the functional significance
443 and molecular mechanisms of proximity-based cell death in CRH neurons.
444 Another extracellular cue that regulates cell death is synaptic transmission, which is
445 critical for neuronal survival during development (Wong and Marin, 2019). In culture,
446 DSCAML1 is localized to excitatory synapses (Yamagata and Sanes, 2010) and inhibits
447 excitatory synaptogenesis when overexpressed (Sachse et al., 2019). Thus, DSCAML1
448 deficiency may increase excitatory synaptic transmission and activation of activity-
449 dependent cell survival pathways (Wong and Marin, 2019). Additionally, increased synaptic

450 excitation has been found to stimulate CRH and AVP expression, which could underlie the
451 increased neuropeptide expression phenotype seen in *dscaml1*-/- animals.

452 **The interplay between cortisol signaling and CRH neuron development**

453 Facilitation and feedback are signature features of the stress axis (Dallman et al., 1992;
454 Spencer and Deak, 2017). While CRH neurons control cortisol levels, cortisol signaling also
455 affects the development of CRH neurons. Zebrafish *gr* mutants have phenotypes similar to
456 that of *dscaml1*-/- animals, including slow visual-background adaptation, sluggish light onset
457 response, elevated cortisol, and increased expression of *crhb* and *pomca* (Griffiths et al., 2012;
458 Muto et al., 2013). Surprisingly, rather than decreased glucocorticoid receptor signaling (as
459 in *gr* mutants), *dscaml1*-/- animals appeared to have enhanced glucocorticoid receptor
460 signaling, with dexamethasone exerting stronger suppression of *crhb* expression and
461 stronger enhancement of *avp* expression. Thus, despite the superficial phenotypic similarity,
462 the underlying signaling mechanisms are distinct between *dscaml1* and *gr* mutants.

463 The diverging response to dexamethasone between *crhb* and *avp* is also intriguing.
464 Mammalian studies have generally found that long-term application of glucocorticoids
465 suppress both *CRH* and *AVP* transcript levels (Watts, 2005). This divergent response to
466 glucocorticoids also makes it less likely that the broad overexpression of stress-related (*crhb,*
467 *pomca, avp, adcyap1b*) and unrelated (*pth2, smtlb, cart3)* neuropeptides are caused by the
468 elevation in cortisol alone. In future work, it will be essential to disambiguate the
469 relationship between cortisol disturbances and developmental deficits. A possible approach
470 would be to normalize cortisol levels by genetically ablating interrenal cells (i.e., genetic
471 adrenalectomy) and supplementing with constant levels of exogenous cortisol (Gutierrez-
472 Triana et al., 2015).

473 **Conclusions**

474 In conclusion, this work shows that DSCAML1 is integral for developing the hypothalamic
475 neurons that regulate the neuroendocrine stress axis. Using zebrafish as a vertebrate model
476 for the ontogenesis of the stress axis, we found that *dscaml1* deficiency results in CRH neuron
477 deficits and the hyperactivation of the stress axis. Genetic perturbations of *DSCAML1* are
478 seen in patients suffering from a wide range of mental health disorders, including intellectual
479 disability, autism spectrum disorder, schizophrenia, epilepsy, and stress disorder (Iossifov
480 et al., 2014; Caramillo et al., 2015; Karaca et al., 2015; Hayase et al., 2020; Ogata et al., 2021;
481 Saadatmand et al., 2021). Developmental deficits in the stress axis may contribute to the
482 etiology of these disorders.

483 **MATERIALS AND METHODS**

484 **Zebrafish Husbandry**

485 Zebrafish (all ages) were raised under a 14/10 light/dark cycle at 28.5°C. Embryos and
486 larvae were raised in E3 buffer (5 mM NaCl, 0.17 mM KCl, 0.33 mM $CaCl_2$, 0.33 mM $MgSO_4$)
487 (Nüsslein-Volhard et al., 2002). All zebrafish used in this study were in a mixed background
488 of AB and TL wild-type strains (Zebrafish International Resource Center). Sex was not a
489 relevant variable for the stages used in this study (0-6 dpf), as laboratory zebrafish remain
490 sexually undifferentiated until two weeks of age (Maack and Segner, 2003; Wilson et al.,
491 2014). All procedures were performed according to protocols approved by the Institutional
492 Animal Care and Use Committee at Virginia Tech and the National Institute for Basic Biology.

493 **Transgenic and mutant zebrafish lines**

494 The *dscaml1*^{vt1} loss-of-function allele contains a 7 base pair deletion that results in
495 premature translational termination (Ma et al., 2020b). Animals used for live imaging were
496 in homozygous *nacre* (*mitfa*) mutant background to prevent pigment formation (Lister et al.,
497 1999). The microglia RFP line [*Tg(mpeg1:Gal4;UAS:NTR-mCherry)*] was obtained from Dr.
498 John Rawls at Duke University (Espenschied et al., 2019). The *crhb:LoxP-RFP-LoxP-GFP* line
499 was generated using CRISPR-mediated knock-in, as described by Kimura et al. (Kimura et al.,
500 2014). The sgRNA sequence for the *crhb* knock-in locus is AGCTCGCGTCTGCGCAGAG.

501 **RNA-seq and differential gene expression analysis**

502 Progenies from heterozygous *dscaml1* mutant parents were anesthetized and harvested
503 at 3.5-4 dpf. The anterior half of the animal was used for RNA preparation using the RNA
504 Miniprep Kit (Zymo). The posterior half was used for genotyping. Three biological replicates
505 for each group were analyzed, each containing RNA from 6-11 animals. All samples had RIN
506 ≥ 8.0 and were converted into a strand-specific library using Illumina's TruSeq Stranded
507 mRNA HT Sample Prep Kit (RS-122-2103; Illumina) for subsequent cluster generation and
508 sequencing on Illumina's NextSeq 75 sequencer. Sequence data processing, alignment, read
509 count, mapping, and quality control were performed as previously described (Ates et al.,
510 2020). Differential expression was tested for significance using the false discovery rate (FDR)
511 (Benjamini-Hochberg) corrected Likelihood Ratio Test (LRT) in the R-package DESeq2 (Love
512 et al., 2014). 238 and 116 genes showed a significant difference in read counts at FDR<0.01
513 and 0.001, respectively. Original sequence data have been deposited in NCBI's Gene
514 Expression Omnibus (Edgar et al., 2002) and will be accessible through GEO Series accession
515 number GSE213858.

516 **Fluorescent *in situ* hybridization and immunohistochemistry**

517 Single and double whole-mount fluorescent *in situ* hybridization (FISH) was performed
518 using protocols described previously (Pan et al., 2012). Probes were synthesized by *in vitro*
519 transcription using the DIG and Fluorescein RNA Labeling Mix (Roche). DIG and fluorescein-
520 labeled probes were detected with anti-DIG or anti-Fluorescein POD-conjugated Fab
521 fragments (Roche) and Cy3 or Fluorescein TSA-plus Reagent (Akoya Biosciences). Plasmid
522 templates for *crhb* (Lohr et al., 2009) and *avp* (Eaton et al., 2008) were provided by Dr. David
523 Prober at Caltech. The *dscaml1* probe was generated as described previously (Ma et al.,
524 2020b).

525 Immunohistochemistry was performed as described previously (Ma et al., 2020a).
526 ERK1/2 was stained with mouse anti-ERK1/2 (4696S; Cell Signaling Technology). Activated
527 caspase 3 was stained with rabbit anti-cleaved caspase 3 (559565; BD Biosciences). Nuclei
528 were stained with TOTO-3 Iodide (ThermoFisher). RFP was stained with chicken anti-RFP
529 (600-901-379S, Rockland) or rabbit anti-RFP (PM005, MBL Life Science). GFP was stained
530 with rabbit anti-GFP (598, MBL Life Science). CRH was stained with rabbit anti-CRH (PBL
531 rC68) provided by P. Sawchenko and J. Vaughan from The Salk Institute. All FISH and
532 immunohistochemistry samples were mounted in 1.5% low-melt agarose in glass-bottomed
533 petri dishes (P50G-1.5-14-F; MatTek) and imaged using a Nikon A1 upright confocal
534 microscope.

535 **Cortisol extraction and ELISA**

536 A detailed protocol for cortisol extraction and ELISA is provided in the online
537 supplementary method. At 4.5 dpf, *dscaml1-/-* and control animals were separated based on
538 the darker pigmentation of the *dscaml1-/-* animal (Ma et al., 2020b). 30-35 animals were

539 placed in each petri dish for cortisol extraction. The morning baseline (unstressed) sample
540 collections were done at 15-30 minutes after light onset (08:15-08:45), and the afternoon
541 sample collections were done between 14:30-16:00. Hyperosmotic stress and stirring stress
542 experiments were done between 14:30-15:30. 6 biological duplicates—each containing a
543 pool of 30 animals—were collected for each genotype (*dscaml1*-/- and control) and stress
544 condition (morning baseline, afternoon baseline, stirring stress, osmotic stress). Mutants
545 and control animals are tested side by side for each experiment.

546 Stirring stress was induced by creating a vortex water flow with a spinning magnetic stir
547 bar (Castillo-Ramirez et al., 2019). A small magnetic stir bar was placed into a 100 mm petri
548 dish containing 35 animals and 20 ml of E3 media. The stir bar was rotated at 300 rpm with
549 a stirring microplate for 5 minutes. Hyperosmotic stress was induced by increasing salt
550 concentration in the media (Yeh et al., 2013). 30 animals were placed in 8 ml of E3 media.
551 Then, 2 ml of prewarmed 1.25M NaCl was added to the media for a final concentration of 250
552 mM for 20 minutes.

553 Sample homogenization and cortisol extraction were performed as described by Yeh et
554 al. (Yeh et al., 2013). Briefly, 5 dpf larvae were rapidly immobilized with ice-cold E3 media
555 and then flash-frozen at -80°C. Once all samples were collected, cortisol from the frozen
556 samples was extracted with ethyl acetate (33211-1L-R; Sigma-Aldrich). Cortisol
557 concentration was measured using a commercial ELISA kit, following the manufacturer's
558 instructions (500360; Cayman Chemical). Sample plates were read with a microplate reader
559 (FilterMax F3; MicroDevices) 90-120 minutes after initial development.

560 **Live imaging of CRH neurons**

561 Cre-mediated recombination of the *crhb:LRLG* transgene was induced by injecting Cre
562 mRNA into the embryo at the 1-cell stage. To achieve partial Cre-mediated recombination,
563 ~30 pg of CreER mRNA was injected at the 1-cell stage and 4-Hydroxytamoxifen (4-OHT)
564 was added to the embryo media at 6 hpf (10 μM), followed by wash out with E3 media at 24
565 hpf. To achieve complete Cre-mediated recombination, ~50 pg of *in vitro* transcribed Cre.zf1
566 mRNA (#61391, Addgene) was injected into the embryos (Horstick et al., 2015).
567 To perform confocal live imaging, 3 dpf animals were anesthetized with 0.01% tricaine
568 methanesulfonate (MS-222, Sigma) and embedded in 1% low-melting point agarose, with
569 the dorsal side resting on the glass surface inside the glass-bottomed petri dish (P50G-1.5-
570 14-F; MatTek) (Beier et al., 2016). The petri dish was then filled with E3 media containing
571 0.01% tricaine methanesulfonate (MS-222, Sigma). Confocal z-stacks were acquired every
572 15 or 30 minutes for 12 hours on a Nikon A1 confocal microscope.
573 Two-photon live imaging was done on a custom Bruker two-channel two-photon
574 microscope. A tuneable Ti:Saphire laser (Chameleon Vision II; Coherent) was tuned to 980
575 nm to excite RFP and GFP simultaneously. 78 hpf animals were anesthetized and embedded
576 the same way as confocal live imaging, but with the dorsal side away from the cover glass.
577 Each animal was imaged at 78, 84, 96, 108, and 120 hpf (Fig. 7A). After each time point,
578 imaged larvae were gently removed from the agarose and recovered in E3 media at 28.5°C
579 under normal day/night cycles. After the last time point, genomic DNA was prepared for all
580 imaged animals and genotyped.

581 **Image Processing and Statistical Analyses**

582 Images were processed using Fiji—an open-source image processing software
583 (Schindelin et al., 2012). For FISH images, images were convolved (kernel=12) to enhance

584 cell boundaries, and the center of each cell was manually tagged using the ROI manager tool.
585 The cell number equals the number of ROIs in each animal. The signal intensity per cell was
586 defined as the median signal intensity of all ROIs in a given animal. The number of contacts
587 for a ROI (cell) is defined as the total number of ROIs within 10 μm, as described previously
588 (Ma et al., 2020b). For each animal, the number of contacts per cell is the mean number of
589 contacts of all ROIs. The number of RFP+ cells in *crhb:LRLG* animals were counted using the
590 ROI manager tool without convolution. For confocal live imaging, images were pre-
591 processed using the Denoise.AI function in the Nikon Elements software. For two-photon
592 imaging, z-stacks from different time points were aligned using the "Correct 3D drift"
593 function. Spectral overlap between the RFP and GFP channels was linearly unmixed.
594 Individual cells were tracked with the MTrackJ plugin in Fiji (Meijering et al., 2012).

595 All statistical analyses were performed in GraphPad Prism (Version 9). For normally-
596 distributed data, parametric tests (*t*-test or ANOVA) were used. For non-normally
597 distributed data, non-parametric tests (Mann-Whitney) were used. The Holm-Sidak post-
598 test was used to correct for multiple comparisons, and the adjusted *p* values were shown. All
599 values are expressed as mean ± standard error. Statistical tests were considered significant
600 when $p<0.05$. Quantification of apoptotic cells was done by the MAP-mapping method, as
601 previously described (Randlett et al., 2015).

602 **AUTHOR CONTRIBUTIONS**

603 M.M and Y.A.P conceived and designed the experiments. M.M and A.A.B prepared samples
604 for RNA sequencing. Y.A.P analyzed the RNA sequencing data. M.M performed ELISA and
605 histochemistry experiments and analyzed the data. M.M and K.C.C performed *in situ*
606 hybridization experiments and analyzed the data with contributions from K.C.C, C.S, and K.S.

607 S.H generated the *crhbl:LRLG* transgenic line. M.M and Y.A.P wrote the manuscript. Y.A.P
608 provided project administration and acquired funding.

609 **ACKNOWLEDGEMENTS**

610 We thank the animal care staff and veterinarians for animal husbandry; members of the
611 Pan laboratory for helpful discussions; R. Settlage for computational analysis of RNA-seq
612 data; S. Ryu and C. Yeh for sharing unpublished data; S. Imani for help with quantification of
613 IHC data; M. Wagle and S. Guo for advice on cortisol extraction procedures; M. Fox and A.
614 Morozov for constructive feedback on the manuscript.

615 **FUNDING**

616 This work was supported by the Commonwealth Research Commercialization Fund
617 (ER14S-001LS to Y.A.P), the Virginia-Maryland College of Veterinary Medicine Intramural
618 Research Fund, the Commonwealth Health Research Board Grant (#208-06-21 to Y.A.P), and
619 funding from Virginia Tech.

620 **DATA AVAILABILITY**

621 Next-generation sequencing data utilized in this publication are available from the Gene
622 Expression Omnibus (accession code GSE213858).

623 **FIGURE LEGENDS**

624 **Fig. 1. Differential gene expression analysis of *dscaml1* deficient zebrafish.** (A) Volcano
625 plot of relative gene expression in *dscaml1-/-* versus control animals. Each dot represents an
626 individual gene, with colored dots representing gene groups as indicated on the graph.
627 Dotted lines show the significance level (adjusted $p < 0.01$) and fold change (increase or

628 decrease by two-fold or more) thresholds. (B, C) Protein class categorization analysis for
629 upregulated (B) and downregulated (C) genes. (D) Table of significantly enriched (*p<0.05*)
630 GO terms for molecular function.

631 **Fig 2. *dscaml1* deficiency alters the development of CRH^{NPO} neurons.** (A) Illustration of
632 CRH neurons (gray circles) in the NPO (boxed area) in the larval zebrafish. (B-B″) Images of
633 double FISH labeling of NPO neurons, with *crhb* labeled in green *avp* in magenta. Arrowhead
634 indicates a cell that expresses *crhb* but not *avp*. (C) Percentage of *crhb+* cells that are *avp+*.
635 n=9. (D) Percentage of *avp+* cells that are *crhb+*. n=9. (E-F″) Developmental trajectory of
636 CRH^{NPO} neurons, labeled by *crhb* FISH. At each developmental stage, a representative
637 confocal z-stack projection of the whole brain is shown in the left panel, and the substack
638 containing the NPO is enlarged and shown in the right panel. The white boxes indicate the
639 locations of the NPO, and the yellow ovals mark the eyes. Wild-type (WT) animals are shown
640 in panels E-E″ and *dscaml1-/-* animals are shown in panels F-F″. (G-I) Quantification of the
641 cell number (G), signal intensity per cell (H), and the number of contacts per cell (I). Multiple-
642 comparison corrected *p* values are as shown. WT: n=9 (2 dpf), 13 (3 dpf), 15(5 dpf). *dscaml1-*
643 */-*: n=9 (2 dpf), 13 (3 dpf), 18 (5 dpf). Scale bars are 20 μm. Mean, standard error, and
644 corrected *p* values are shown for all graphs.

645 **Fig 3. *dscaml1* deficiency alters the development of CRH$^{NPO\text{-}AVP}$ neurons.** (A-B″)
646 Developmental trajectory of CRH$^{NPO\text{-}AVP}$ neurons, labeled by *avp* FISH. At each developmental
647 stage, a representative confocal z-stack projection of the whole brain is shown in the left
648 panel, and the substack containing the NPO is enlarged and shown in the right panel. The
649 white boxes indicate the locations of the NPO, and the yellow ovals mark the eyes. Wild-type
650 (WT) animals are shown in panels A-A″ and *dscaml1-/-* animals are shown in panels B-B″.

651 (C-E) Quantification of the cell number (C), signal intensity per cell (D), and the number of
652 contacts per cell (E). Multiple-comparison corrected *p* values are as shown. WT: n=9 (2 dpf),
653 15 (3 dpf), 14(5 dpf). *dscaml1-/-*: n=9 (2 dpf), 15 (3 dpf), 20 (5 dpf). Scale bars are 20 μm.
654 Mean, standard error, and corrected *p* values are shown for all graphs.

655 **Fig 4. CRH^{NPO} neuron development is impaired in the absence of ambient light.** (A-C)
656 Quantification of CRH^{NPO} neurons, labeled by *crhb* FISH. Graphs show the cell number (A),
657 signal intensity per cell (B), and the number of contacts per cell (C). Multiple-comparison
658 corrected *p* values are as shown. WT: n=10 (3 dpf), 15 (5 dpf). *dscaml1-/-*: n=17 (3 dpf), 15
659 (5 dpf). (D-F) Quantification of CRH$^{NPO-AVP}$ neurons, labeled by *avp* FISH. Graphs show the
660 cell number (D), signal intensity per cell (E), and the number of contacts per cell (F).
661 Multiple-comparison corrected *p* values are as shown. WT: n=15 (3 dpf), 11 (5 dpf). *dscaml1-*
662 */-*: n=15 (3 dpf), 11 (5 dpf). Mean, standard error, and corrected *p* values are shown for all
663 graphs.

664 **Fig. 5. Fluorescent labeling and live imaging of CRH^{NPO} neurons.** (A) Schematic of CRISPR
665 -mediated knock-in of the *hsp-Lox-RFP-Lox-GFP* cassette at the sgRNA target site, located 35
666 bp upstream of exon 1 of *crhb*. The orientation and junctional structure of insertion have not
667 been determined. (B) Schematic of *crhb:LRLG* expression. Each circle represents a
668 fluorescent cell. Without Cre (default), RFP is expressed in all cells. With full recombination,
669 all cells express GFP. Partial recombination results in mosaic RFP and GFP labeling. (C)
670 Dorsal view of a fixed 5 dpf *crhb:LRLG* larvae with partial recombination stained with anti-
671 RFP (magenta) and anti-GFP (green). The boxed area marks the NPO. (D) Higher
672 magnification image of the NPO. Both RFP and GFP-positive neurons can be seen. (E-F′)
673 Images of anti-RFP stained *crh:LRLG* animals without recombination. Representative wild-

674 type (WT, E-E′) and *dscaml1-/-* (F-F′) NPO neurons are shown. (G) Quantification of RFP-
675 positive cells at 3 and 5 dpf. WT: n=5 (3 dpf), 16 (5 dpf). *dscaml1-/-*: n=11 (3 dpf), 17 (5 dpf).
676 Mean, standard error, and corrected *p* values are shown. (H-H″) Live *crhb:LRLG* larvae with
677 partial recombination were imaged from 72 to 84 hpf. Three time points are shown here.
678 Two cells (arrowheads, one green and one magenta) move away over time. (I-I″) Live
679 *crhb:LRLG;mpeg1:Gal4;UAS:NTR-mCherry* larvae with CRH neurons labeled with GFP (green)
680 and microglia labeled with mCherry (magenta). In this image series, one CRH neuron
681 (arrowhead) is engulfed (I′) and then removed (I″) by a microglial cell. Images are confocal
682 optical sections. (J-J′) Panels showing enlarged views of the boxed area in I″, with (J) or
683 without (J′) the mCherry channel. The remnant of the CRH neuron can still be seen inside the
684 microglia (arrowheads). Scale bars are 100 μm (panel C) or 20 μm (all other images).

685 **Fig. 6. Live tracking of CRH^{NPO} neuron cell fate.** (A) Timeline of time-lapse two-photon (2P)
686 imaging experiment. Partial recombination of *crhb:LRLG* was induced by 4-OHT at 6-24 hpf,
687 and imaging was performed at 78, 84, 96, 108, and 120 hpf. Animals were briefly
688 anesthetized during imaging and allowed to recover in between imaging sessions. (B-B″)
689 Tracking of individual CRH^{NPO} neurons. Three example time frames are shown. Individual
690 fluorescent cells can be tracked over time and are divided into two categories: persisting
691 (white arrows) or lost (pink arrow). (C) Quantification of the percentage of persisting versus
692 lost CRH^{NPO} neurons. Sample size (cell number) as indicated for each genotype. (D) Survival
693 curve of individual CRH^{NPO} neurons in each genotypic group.

694 **Fig. 7. Cortisol levels, response to exogenous glucocorticoids, and summary of findings.**
695 (A) Cortisol profile for 5 dpf larvae. For each sample (dot), cortisol was extracted from a pool
696 of 30 animals. n=6 for all groups. Median, interquartile range, and corrected *p* values are

697 shown. (B) Quantification of *crhb* signal intensity per cell in CRH^{NPO} neurons. Vehicle: n=10
698 (WT), 11 (*dscaml1-/-*). Dex: n=7 (WT), 11 (*dscaml1-/-*). Mean, standard error, and corrected
699 *p* values are shown. (C) Quantification of *avp* signal intensity per cell in $CRH^{NPO\text{-}AVP}$ neurons.
700 Vehicle: n=8 (WT), 12 (*dscaml1-/-*). Dex: n=9 (WT), 10 (*dscaml1-/-*). Mean, standard error,
701 and corrected *p* values are shown. (D) Schematic summary of findings. CRH^{NPO} neurons are
702 formed normally early on (2 dpf) but begin to exhibit developmental abnormalities in
703 *dscaml1* deficient animals. The developmental deficits collectively contribute to the
704 hyperactive stress axis and attenuated acute stress response in *dscaml1* mutants.

705 **Supplementary Fig. 1. *dscaml1* is expressed in CRH^{NPO} neurons during larval**
706 **development.** (A-B″) Double FISH with *crhb* (green) and *dscaml1* (magenta) RNA probes at
707 2 (A-A″) and 5 dpf (B-B″). Arrowheads mark *crhb*+ cells that co-express *dscaml1*. Scale bars
708 are 20 μm.

709 **Supplementary Fig. 2. Programmed cell death in the brain is reduced in *dscaml1***
710 **mutants.** (A-B″) Immunolabeling with anti-AC3 (green) and counterstained with anti-
711 ERK1/2 (magenta). 1 dpf embryos are shown laterally, and 3 and 5 dpf larvae dorsally. Wild-
712 type (WT) animals are shown in panels A-A″ and *dscaml1-/-* animals are shown in panels B-
713 B″. (C) 5 dpf Z-Brain mapping of brain regions (dorsal view), showing regions with higher
714 AC3 labeling in wild type (green) or *dscaml1-/-* (magenta). (D) Summary graph of the top
715 regions where wild-type animals had more AC3 labeling than *dscaml1-/-* animals. Anterior
716 is to the left for all images. Scale bars are 100 μm.

717 **Supplementary Fig. 3. The *crhb:LRLG* transgenic line labels CRH-expressing neurons.**
718 (A-A″) Most RFP+ neurons (magenta, anti-RFP) express the CRH protein (green, anti-CRH).

719 (B) Percentage of RFP+ neurons that express CRH. Mean, standard error, and sample size
720 are shown. The scale bar is 20 μm.

721 **Supplementary Video 1.** Time-lapse movie of *crhb:LRLG* larvae. CRH neurons were labeled
722 with RFP (magenta) and GFP (green). Two cells (arrowheads, one green and one magenta),
723 the same ones as shown in Fig. 5H-H″, move away over time.

724 **Supplementary Video 2.** Time-lapse movie of *crhb:LRLG;mpeg1:Gal4;UAS:NTR-mCherry*
725 larvae with CRH neurons labeled with GFP (green) and microglia labeled with mCherry
726 (magenta). The red "X" marks the cell indicated in Fig. 5I-J′. Maximum projection of z-stack
727 for each time point is shown.

728 **REFERENCES**

729 Alderman SL, Bernier NJ (2009) Ontogeny of the corticotropin-releasing factor system in zebrafish.
730 Gen Comp Endocrinol 164:61-69.
731 Alsop D, Vijayan MM (2008) Development of the corticosteroid stress axis and receptor expression
732 in zebrafish. Am J Physiol Regul Integr Comp Physiol 294:R711-719.
733 Alsop D, Vijayan M (2009) The zebrafish stress axis: molecular fallout from the teleost-specific
734 genome duplication event. Gen Comp Endocrinol 161:62-66.
735 Alvarez-Bolado G (2019) Development of neuroendocrine neurons in the mammalian hypothalamus.
736 Cell Tissue Res 375:23-39.
737 Arnett MG, Muglia LM, Laryea G, Muglia LJ (2016) Genetic Approaches to Hypothalamic-Pituitary-
738 Adrenal Axis Regulation. Neuropsychopharmacology 41:245-260.
739 Ates KM, Wang T, Moreland T, Veeranan-Karmegam R, Ma M, Jeter C, Anand P, Wenzel W, Kim HG,
740 Wolfe LA, Stephen J, Adams DR, Markello T, Tifft CJ, Settlage R, Gahl WA, Gonsalvez GB,
741 Malicdan MC, Flanagan-Steet H, Pan YA (2020) Deficiency in the endocytic adaptor proteins
742 PHETA1/2 impairs renal and craniofacial development. Disease models & mechanisms 13.
743 Bai Y, Liu H, Huang B, Wagle M, Guo S (2016) Identification of environmental stressors and validation
744 of light preference as a measure of anxiety in larval zebrafish. BMC neuroscience 17:63.
745 Beier KT, Mundell NA, Pan YA, Cepko CL (2016) Anterograde or Retrograde Transsynaptic Circuit
746 Tracing in Vertebrates with Vesicular Stomatitis Virus Vectors. Curr Protoc Neurosci 74:1 26
747 21-21 26 27.
748 Caramillo EM, Khan KM, Collier AD, Echevarria DJ (2015) Modeling PTSD in the zebrafish: are we
749 there yet? Behav Brain Res 276:151-160.
750 Castillo-Ramirez LA, Ryu S, De Marco RJ (2019) Active behaviour during early development shapes
751 glucocorticoid reactivity. Sci Rep 9:12796.
752 Chen SK, Chew KS, McNeill DS, Keeley PW, Ecker JL, Mao BQ, Pahlberg J, Kim B, Lee SC, Fox MA, Guido
753 W, Wong KY, Sampath AP, Reese BE, Kuruvilla R, Hattar S (2013) Apoptosis regulates ipRGC
754 spacing necessary for rods and cones to drive circadian photoentrainment. Neuron 77:503-
755 515.

756 Chen Y, Baram TZ (2016) Toward Understanding How Early-Life Stress Reprograms Cognitive and
757 Emotional Brain Networks. Neuropsychopharmacology 41:197-206.
758 Clark KJ, Boczek NJ, Ekker SC (2011) Stressing zebrafish for behavioral genetics. Reviews in the
759 neurosciences 22:49-62.
760 Cole LK, Ross LS (2001) Apoptosis in the developing zebrafish embryo. Dev Biol 240:123-142.
761 Dallman MF, Akana SF, Scribner KA, Bradbury MJ, Walker CD, Strack AM, Cascio CS (1992) Stress,
762 Feedback and Facilitation in the Hypothalamo-Pituitary-Adrenal Axis. J Neuroendocrinol
763 4:517-526.
764 Denver RJ (2009) Structural and functional evolution of vertebrate neuroendocrine stress systems.
765 Ann N Y Acad Sci 1163:1-16.
766 Eaton JL, Holmqvist B, Glasgow E (2008) Ontogeny of vasotocin-expressing cells in zebrafish:
767 selective requirement for the transcriptional regulators orthopedia and single-minded 1 in
768 the preoptic area. Dev Dyn 237:995-1005.
769 Espenschied S, T., Cronan Mark R, Matty Molly A, Mueller O, Redinbo Matthew R, Tobin David M,
770 Rawls John F (2019) Epithelial delamination is protective during pharmaceutical-induced
771 enteropathy. Proceedings of the National Academy of Sciences 116:16961-16970.
772 Forger NG (2009) Control of cell number in the sexually dimorphic brain and spinal cord. J
773 Neuroendocrinol 21:393-399.
774 Fuerst PG, Bruce F, Tian M, Wei W, Elstrott J, Feller MB, Erskine L, Singer JH, Burgess RW (2009)
775 DSCAM and DSCAML1 function in self-avoidance in multiple cell types in the developing
776 mouse retina. Neuron 64:484-497.
777 Garrett AM, Tadenev AL, Burgess RW (2012) DSCAMs: restoring balance to developmental forces.
778 Frontiers in molecular neuroscience 5:86.
779 Garrett AM, Tadenev AL, Hammond YT, Fuerst PG, Burgess RW (2016) Replacing the PDZ-interacting
780 C-termini of DSCAM and DSCAML1 with epitope tags causes different phenotypic severity in
781 different cell populations. eLife 5.
782 Griffiths BB, Schoonheim PJ, Ziv L, Voelker L, Baier H, Gahtan E (2012) A zebrafish model of
783 glucocorticoid resistance shows serotonergic modulation of the stress response. Front Behav
784 Neurosci 6:68.
785 Gutierrez-Triana JA, Herget U, Castillo-Ramirez LA, Lutz M, Yeh CM, De Marco RJ, Ryu S (2015)
786 Manipulation of Interrenal Cell Function in Developing Zebrafish Using Genetically Targeted
787 Ablation and an Optogenetic Tool. Endocrinology 156:3394-3401.
788 Hayase Y et al. (2020) Down syndrome cell adhesion molecule like-1 (DSCAML1) links the GABA
789 system and seizure susceptibility. Acta Neuropathologica Communications 8:206.
790 Herget U, Ryu S (2015) Coexpression analysis of nine neuropeptides in the neurosecretory preoptic
791 area of larval zebrafish. Front Neuroanat 9:2.
792 Hooper A, Paracha R, Maguire J (2018) Seizure-induced activation of the HPA axis increases seizure
793 frequency and comorbid depression-like behaviors. Epilepsy & behavior : E&B 78:124-133.
794 Horstick EJ, Jordan DC, Bergeron SA, Tabor KM, Serpe M, Feldman B, Burgess HA (2015) Increased
795 functional protein expression using nucleotide sequence features enriched in highly
796 expressed genes in zebrafish. Nucleic acids research 43:e48.
797 Iossifov I et al. (2014) The contribution of de novo coding mutations to autism spectrum disorder.
798 Nature 515:216-221.
799 Irles C, Nava-Kopp AT, Morán J, Zhang L (2014) Neonatal maternal separation up-regulates protein
800 signalling for cell survival in rat hypothalamus. Stress 17:275-284.
801 Karaca E et al. (2015) Genes that Affect Brain Structure and Function Identified by Rare Variant
802 Analyses of Mendelian Neurologic Disease. Neuron 88:499-513.
803 Keeley PW, Sliff BJ, Lee SC, Fuerst PG, Burgess RW, Eglen SJ, Reese BE (2012) Neuronal clustering and
804 fasciculation phenotype in Dscam- and Bax-deficient mouse retinas. J Comp Neurol
805 520:1349-1364.

806 Keen-Rhinehart E, Michopoulos V, Toufexis DJ, Martin EI, Nair H, Ressler KJ, Davis M, Owens MJ,
807 Nemeroff CB, Wilson ME (2009) Continuous expression of corticotropin-releasing factor in
808 the central nucleus of the amygdala emulates the dysregulation of the stress and reproductive
809 axes. Molecular psychiatry 14:37-50.
810 Kimmel CB, Ballard WW, Kimmel SR, Ullmann B, Schilling TF (1995) Stages of embryonic
811 development of the zebrafish. Dev Dyn 203:253-310.
812 Kimura Y, Hisano Y, Kawahara A, Higashijima S (2014) Efficient generation of knock-in transgenic
813 zebrafish carrying reporter/driver genes by CRISPR/Cas9-mediated genome engineering. Sci
814 Rep 4:6545.
815 Kolber BJ, Boyle MP, Wieczorek L, Kelley CL, Onwuzurike CC, Nettles SA, Vogt SK, Muglia LJ (2010)
816 Transient early-life forebrain corticotropin-releasing hormone elevation causes long-lasting
817 anxiogenic and despair-like changes in mice. J Neurosci 30:2571-2581.
818 Lister JA, Robertson CP, Lepage T, Johnson SL, Raible DW (1999) nacre encodes a zebrafish
819 microphthalmia-related protein that regulates neural-crest-derived pigment cell fate.
820 Development 126:3757-3767.
821 Lohr H, Hammerschmidt M (2011) Zebrafish in endocrine systems: recent advances and implications
822 for human disease. Annu Rev Physiol 73:183-211.
823 Lohr H, Ryu S, Driever W (2009) Zebrafish diencephalic A11-related dopaminergic neurons share a
824 conserved transcriptional network with neuroendocrine cell lineages. Development
825 136:1007-1017.
826 Love MI, Huber W, Anders S (2014) Moderated estimation of fold change and dispersion for RNA-seq
827 data with DESeq2. Genome Biology 15:550.
828 Lovett-Barron M, Chen R, Bradbury S, Andalman AS, Wagle M, Guo S, Deisseroth K (2020) Multiple
829 convergent hypothalamus-brainstem circuits drive defensive behavior. Nat Neurosci 23:959-
830 967.
831 Ma M, Kler S, Pan YA (2020a) Structural Neural Connectivity Analysis in Zebrafish With Restricted
832 Anterograde Transneuronal Viral Labeling and Quantitative Brain Mapping. Frontiers in
833 neural circuits 13:85.
834 Ma M, Ramirez AD, Wang T, Roberts RL, Harmon KE, Schoppik D, Sharma A, Kuang C, Goei SL, Gagnon
835 JA, Zimmerman S, Tsai SQ, Reyon D, Joung JK, Aksay ERF, Schier AF, Pan YA (2020b) Zebrafish
836 *dscaml1* Deficiency Impairs Retinal Patterning and Oculomotor Function. J Neurosci 40:143-
837 158.
838 Maack G, Segner H (2003) Morphological development of the gonads in zebrafish. Journal of Fish
839 Biology 62:895-906.
840 Mazaheri F, Breus O, Durdu S, Haas P, Wittbrodt J, Gilmour D, Peri F (2014) Distinct roles for BAI1
841 and TIM-4 in the engulfment of dying neurons by microglia. Nature communications 5:4046.
842 McEwen BS, Akil H (2020) Revisiting the Stress Concept: Implications for Affective Disorders. J
843 Neurosci 40:12-21.
844 Meijering E, Dzyubachyk O, Smal I (2012) Methods for cell and particle tracking. Methods Enzymol
845 504:183-200.
846 Merali Z, Kent P, Du L, Hrdina P, Palkovits M, Faludi G, Poulter MO, Bedard T, Anisman H (2006)
847 Corticotropin-releasing hormone, arginine vasopressin, gastrin-releasing peptide, and
848 neuromedin B alterations in stress-relevant brain regions of suicides and control subjects.
849 Biological psychiatry 59:594-602.
850 Mi H, Ebert D, Muruganujan A, Mills C, Albou L-P, Mushayamaha T, Thomas PD (2021) PANTHER
851 version 16: a revised family classification, tree-based classification tool, enhancer regions and
852 extensive API. Nucleic acids research 49:D394-D403.
853 Moreland T, Poulain FE (2022) To Stick or Not to Stick: The Multiple Roles of Cell Adhesion Molecules
854 in Neural Circuit Assembly. Frontiers in Neuroscience 16.

855 Muto A, Taylor MR, Suzawa M, Korenbrot JI, Baier H (2013) Glucocorticoid receptor activity regulates
856 light adaptation in the zebrafish retina. Frontiers in neural circuits 7:145.
857 Nagpal J, Herget U, Choi MK, Ryu S (2019) Anatomy, development, and plasticity of the
858 neurosecretory hypothalamus in zebrafish. Cell Tissue Res 375:5-22.
859 Nemeroff CB, Widerlov E, Bissette G, Walleus H, Karlsson I, Eklund K, Kilts CD, Loosen PT, Vale W
860 (1984) Elevated concentrations of CSF corticotropin-releasing factor-like immunoreactivity
861 in depressed patients. Science 226:1342-1344.
862 Nüsslein-Volhard C, Gilmour D, Dahm R (2002) Introduction: zebrafish as a system to study
863 development and organogenesis. Zebrafish: a practical approach:1-5.
864 O'Toole KK, Hooper A, Wakefield S, Maguire J (2014) Seizure-induced disinhibition of the HPA axis
865 increases seizure susceptibility. Epilepsy research 108:29-43.
866 Ogata S, Hashizume K, Hayase Y, Kanno Y, Hori K, Balan S, Yoshikawa T, Takahashi H, Taya S, Hoshino
867 M (2021) Potential involvement of DSCAML1 mutations in neurodevelopmental disorders.
868 Genes to Cells 26:136-151.
869 Pan YA, Choy M, Prober DA, Schier AF (2012) Robo2 determines subtype-specific axonal projections
870 of trigeminal sensory neurons. Development 139:591-600.
871 Placzek M, Fu T, Towers M (2020) Development of the Neuroendocrine Hypothalamus. In:
872 Developmental Neuroendocrinology (Wray S, Blackshaw S, eds), pp 3-30. Cham: Springer
873 International Publishing.
874 Raadsheer FC, van Heerikhuize JJ, Lucassen PJ, Hoogendijk WJ, Tilders FJ, Swaab DF (1995)
875 Corticotropin-releasing hormone mRNA levels in the paraventricular nucleus of patients with
876 Alzheimer's disease and depression. Am J Psychiatry 152:1372-1376.
877 Randlett O, Wee CL, Naumann EA, Nnaemeka O, Schoppik D, Fitzgerald JE, Portugues R, Lacoste AM,
878 Riegler C, Engert F, Schier AF (2015) Whole-brain activity mapping onto a zebrafish brain
879 atlas. Nat Methods 12:1039-1046.
880 Regev L, Baram TZ (2014) Corticotropin releasing factor in neuroplasticity. Front Neuroendocrinol
881 35:171-179.
882 René P, Grino M, Viollet C, Videau C, Jullian E, Bucchini D, Epelbaum J, Bertagna X, De Keyzer Y (2002)
883 Overexpression of the V3 Vasopressin Receptor in Transgenic Mice Corticotropes Leads to
884 Increased Basal Corticosterone. J Neuroendocrinol 14:737-744.
885 Romanov RA, Alpar A, Hokfelt T, Harkany T (2017) Molecular diversity of corticotropin-releasing
886 hormone mRNA-containing neurons in the hypothalamus. J Endocrinol 232:R161-R172.
887 Saadatmand F, Gurdziel K, Jackson L, Kwabi-Addo B, Ruden DM (2021) DNA methylation and
888 exposure to violence among African American young adult males. Brain, Behavior, &
889 Immunity - Health 14:100247.
890 Sachse SM, Lievens S, Ribeiro LF, Dascenco D, Masschaele D, Horre K, Misbaer A, Vanderroost N, De
891 Smet AS, Salta E, Erfurth ML, Kise Y, Nebel S, Van Delm W, Plaisance S, Tavernier J, De Strooper
892 B, De Wit J, Schmucker D (2019) Nuclear import of the DSCAM-cytoplasmic domain drives
893 signaling capable of inhibiting synapse formation. EMBO J 38.
894 Sanes JR, Zipursky SL (2020) Synaptic Specificity, Recognition Molecules, and Assembly of Neural
895 Circuits. Cell 181:536-556.
896 Schindelin J, Arganda-Carreras I, Frise E, Kaynig V, Longair M, Pietzsch T, Preibisch S, Rueden C,
897 Saalfeld S, Schmid B, Tinevez JY, White DJ, Hartenstein V, Eliceiri K, Tomancak P, Cardona A
898 (2012) Fiji: an open-source platform for biological-image analysis. Nat Methods 9:676-682.
899 Short AK, Thai CW, Chen Y, Kamei N, Pham AL, Birnie MT, Bolton JL, Mortazavi A, Baram TZ (2021)
900 Single-Cell Transcriptional Changes in Hypothalamic Corticotropin-Releasing Factor–
901 Expressing Neurons After Early-Life Adversity Inform Enduring Alterations in Vulnerabilities
902 to Stress. Biological Psychiatry Global Open Science.
903 Simerly RB (2002) Wired for reproduction: organization and development of sexually dimorphic
904 circuits in the mammalian forebrain. Annu Rev Neurosci 25:507-536.

905 Spencer RL, Deak T (2017) A users guide to HPA axis research. Physiol Behav 178:43-65.
906 Stenzel-Poore MP, Cameron VA, Vaughan J, Sawchenko PE, Vale W (1992) Development of Cushing's
907 syndrome in corticotropin-releasing factor transgenic mice. Endocrinology 130:3378-3386.
908 Stroth N, Holighaus Y, Ait-Ali D, Eiden LE (2011) PACAP: a master regulator of neuroendocrine stress
909 circuits and the cellular stress response. Annals of the New York Academy of Sciences
910 1220:49-59.
911 van Bodegom M, Homberg JR, Henckens M (2017) Modulation of the Hypothalamic-Pituitary-Adrenal
912 Axis by Early Life Stress Exposure. Front Cell Neurosci 11:87.
913 Watts AG (2005) Glucocorticoid regulation of peptide genes in neuroendocrine CRH neurons: A
914 complexity beyond negative feedback. Frontiers in Neuroendocrinology 26:109-130.
915 Wendelaar Bonga SE (1997) The stress response in fish. Physiol Rev 77:591-625.
916 Wilson CA, High SK, McCluskey BM, Amores A, Yan YL, Titus TA, Anderson JL, Batzel P, Carvan MJ, 3rd,
917 Schartl M, Postlethwait JH (2014) Wild sex in zebrafish: loss of the natural sex determinant
918 in domesticated strains. Genetics 198:1291-1308.
919 Wong FK, Marin O (2019) Developmental Cell Death in the Cerebral Cortex. Annu Rev Cell Dev Biol
920 35:523-542.
921 Yamagata M, Sanes JR (2008) Dscam and Sidekick proteins direct lamina-specific synaptic
922 connections in vertebrate retina. Nature 451:465-469.
923 Yamagata M, Sanes JR (2010) Synaptic localization and function of Sidekick recognition molecules
924 require MAGI scaffolding proteins. J Neurosci 30:3579-3588.
925 Yamaguchi Y, Miura M (2015) Programmed cell death in neurodevelopment. Dev Cell 32:478-490.
926 Yeh CM, Glock M, Ryu S (2013) An optimized whole-body cortisol quantification method for assessing
927 stress levels in larval zebrafish. PLoS One 8:e79406.
928 Zhang L, Hernández VS, Liu B, Medina MP, Nava-Kopp AT, Irles C, Morales M (2012) Hypothalamic
929 vasopressin system regulation by maternal separation: its impact on anxiety in rats.
930 Neuroscience 215:135-148.
931 Ziv L, Muto A, Schoonheim PJ, Meijsing SH, Strasser D, Ingraham HA, Schaaf MJ, Yamamoto KR, Baier
932 H (2013) An affective disorder in zebrafish with mutation of the glucocorticoid receptor.
933 Molecular psychiatry 18:681-691.
934

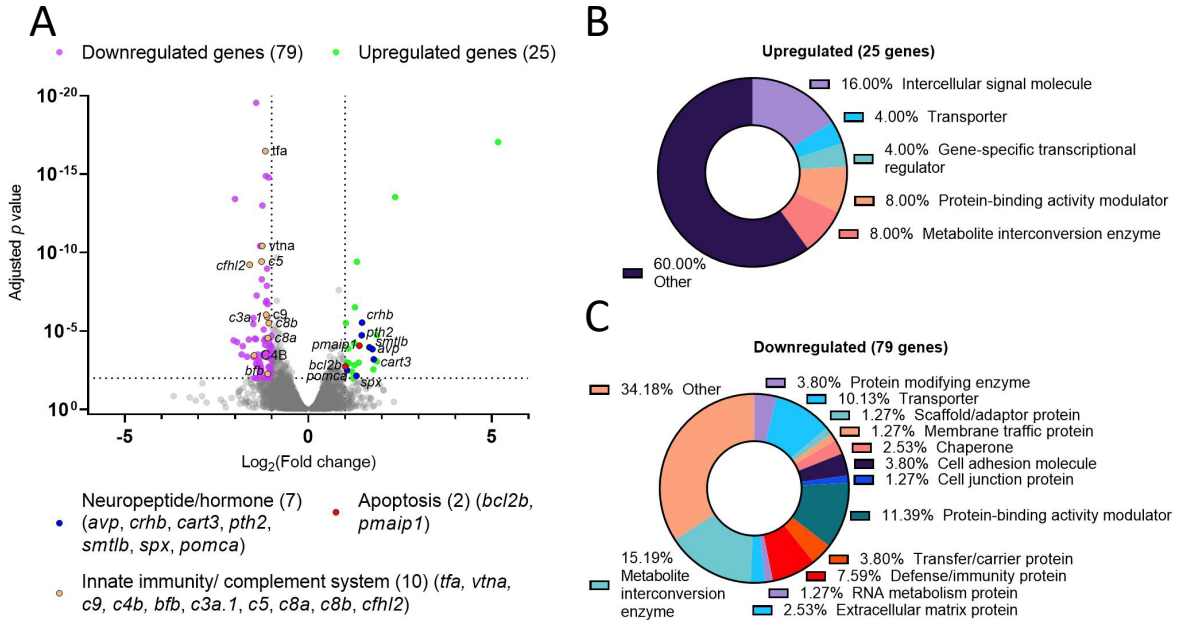

D

GO molecular function (complete)	Number of genes	Over (+) /Under(-)	*p* value
hormone activity (GO:0005179)	8	+	4.40E-05
signaling receptor activator activity (GO:0030546)	10	+	6.19E-06
signaling receptor regulator activity (GO:0030545)	10	+	6.19E-06
receptor ligand activity (GO:0048018)	10	+	6.19E-06

Figure 1

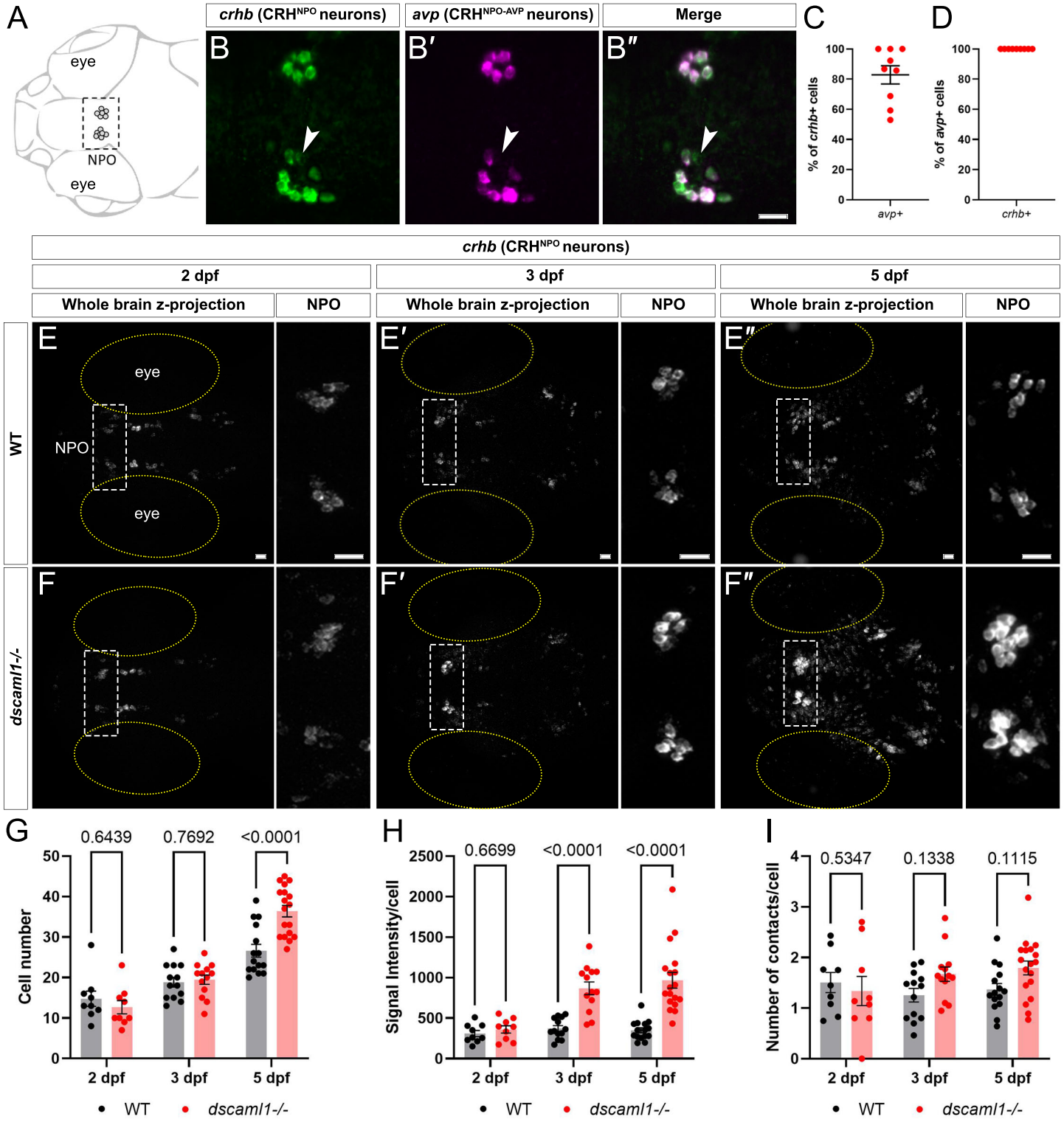
A
eye
NPO
eye
crhb (CRHNPO neurons)
avp (CRHNPO-AVP neurons)
Merge
B
B′
B″
C
D
% of crhb+ cells
% of avp+ cells
avp+
crhb+
crhb (CRHNPO neurons)
2 dpf
3 dpf
5 dpf
Whole brain z-projection
NPO
WT
dscaml1-/-
E
E′
E″
F
F′
F″
eye
NPO
eye
G
H
I
Cell number
Signal Intensity/cell
Number of contacts/cell
0.6439
0.7692
<0.0001
0.6699
<0.0001
<0.0001
0.5347
0.1338
0.1115
2 dpf
3 dpf
5 dpf
WT
dscaml1-/-

Figure 2

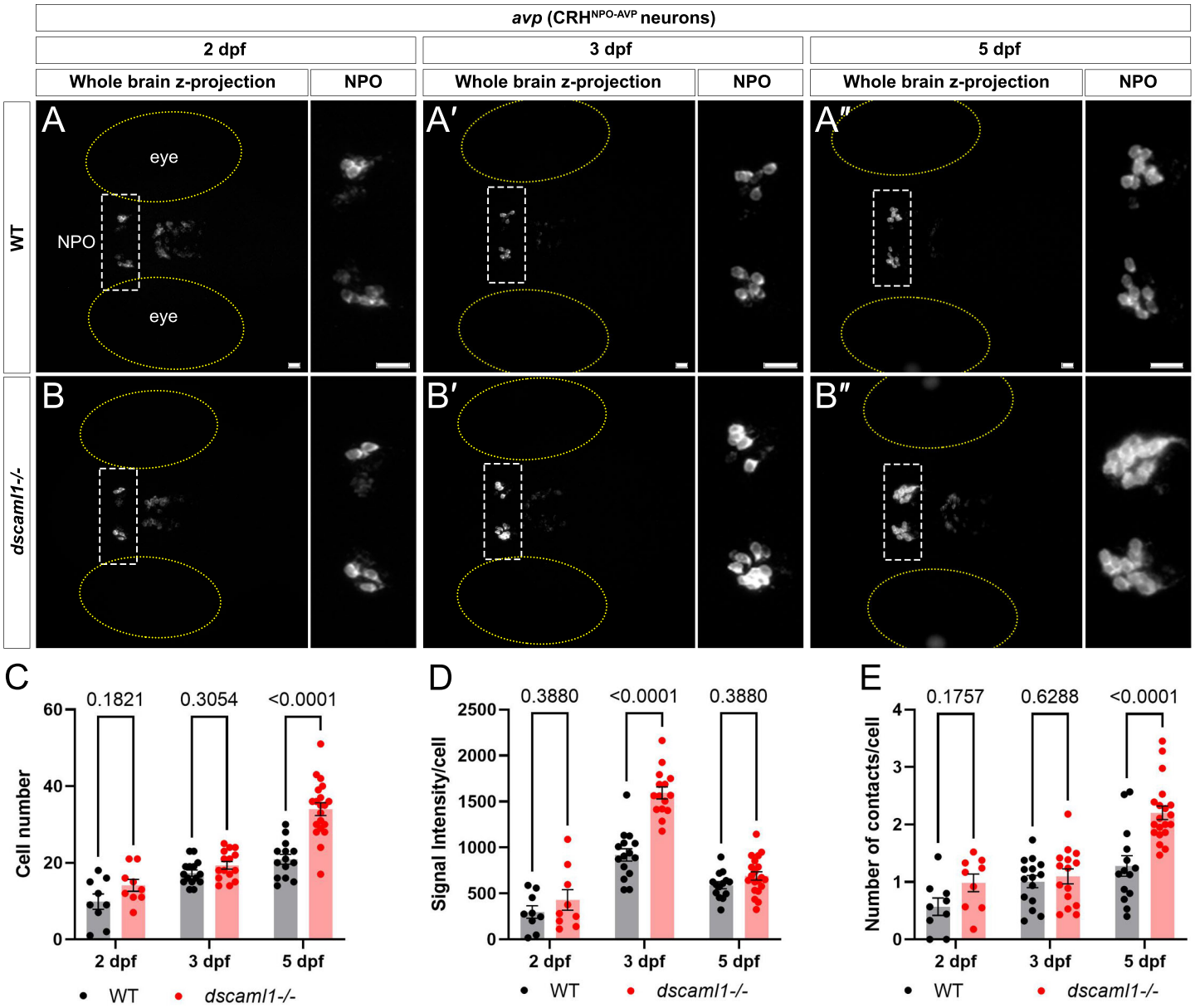
avp (CRHNPO-AVP neurons)
2 dpf
3 dpf
5 dpf
Whole brain z-projection
NPO
WT
dscaml1-/-
A
A′
A″
B
B′
B″
eye
NPO
eye
C
D
E
0.1821
0.3054
<0.0001
0.3880
<0.0001
0.3880
0.1757
0.6288
<0.0001
Cell number
Signal Intensity/cell
Number of contacts/cell
2 dpf
3 dpf
5 dpf
WT
dscaml1-/-

Figure 3

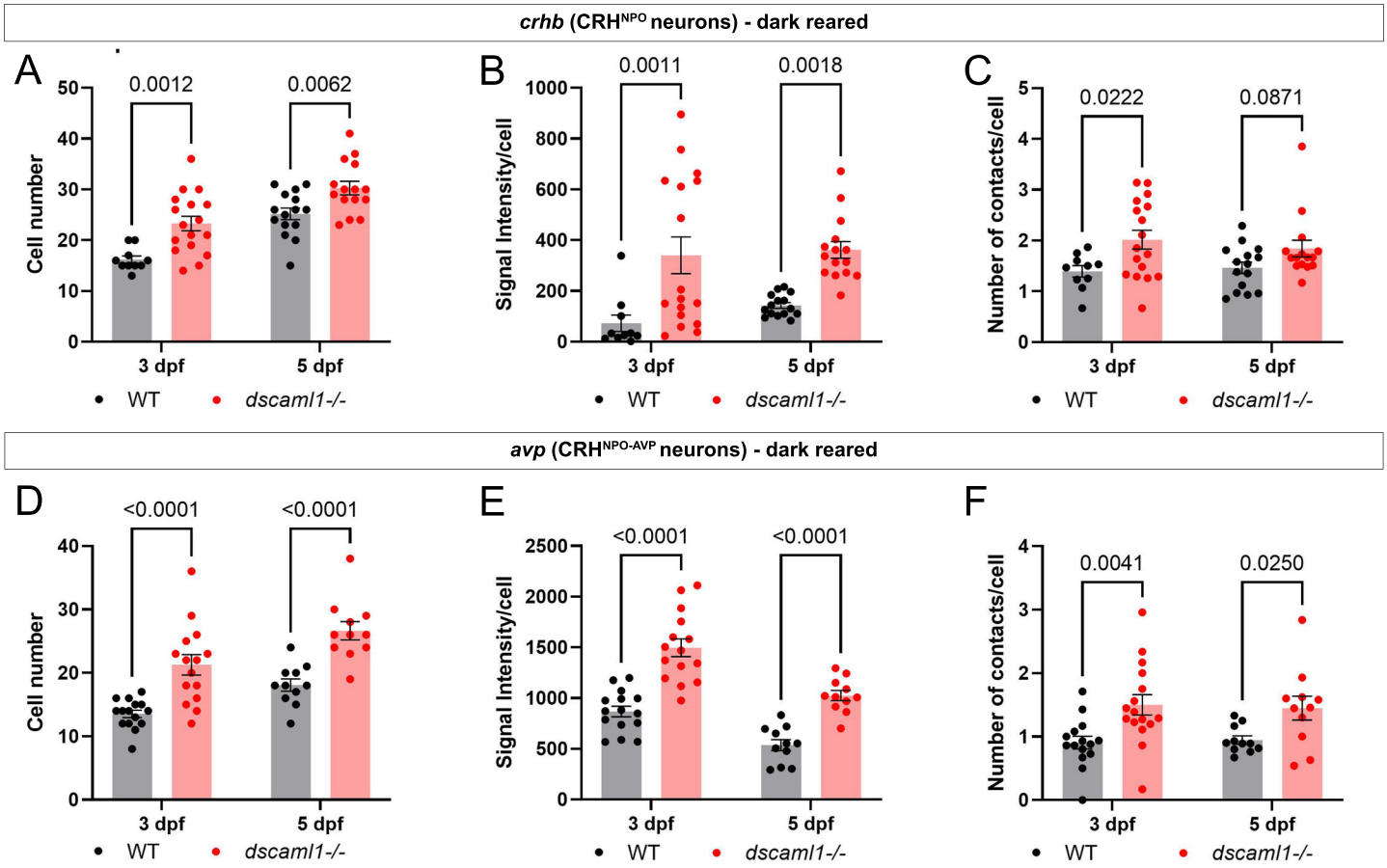
crhb (CRHNPO neurons) - dark reared
A
0.0012
0.0062
Cell number
3 dpf
5 dpf
WT
dscaml1-/-
B
0.0011
0.0018
Signal Intensity/cell
C
0.0222
0.0871
Number of contacts/cell
avp (CRHNPO-AVP neurons) - dark reared
D
<0.0001
<0.0001
E
<0.0001
<0.0001
F
0.0041
0.0250

Figure 4

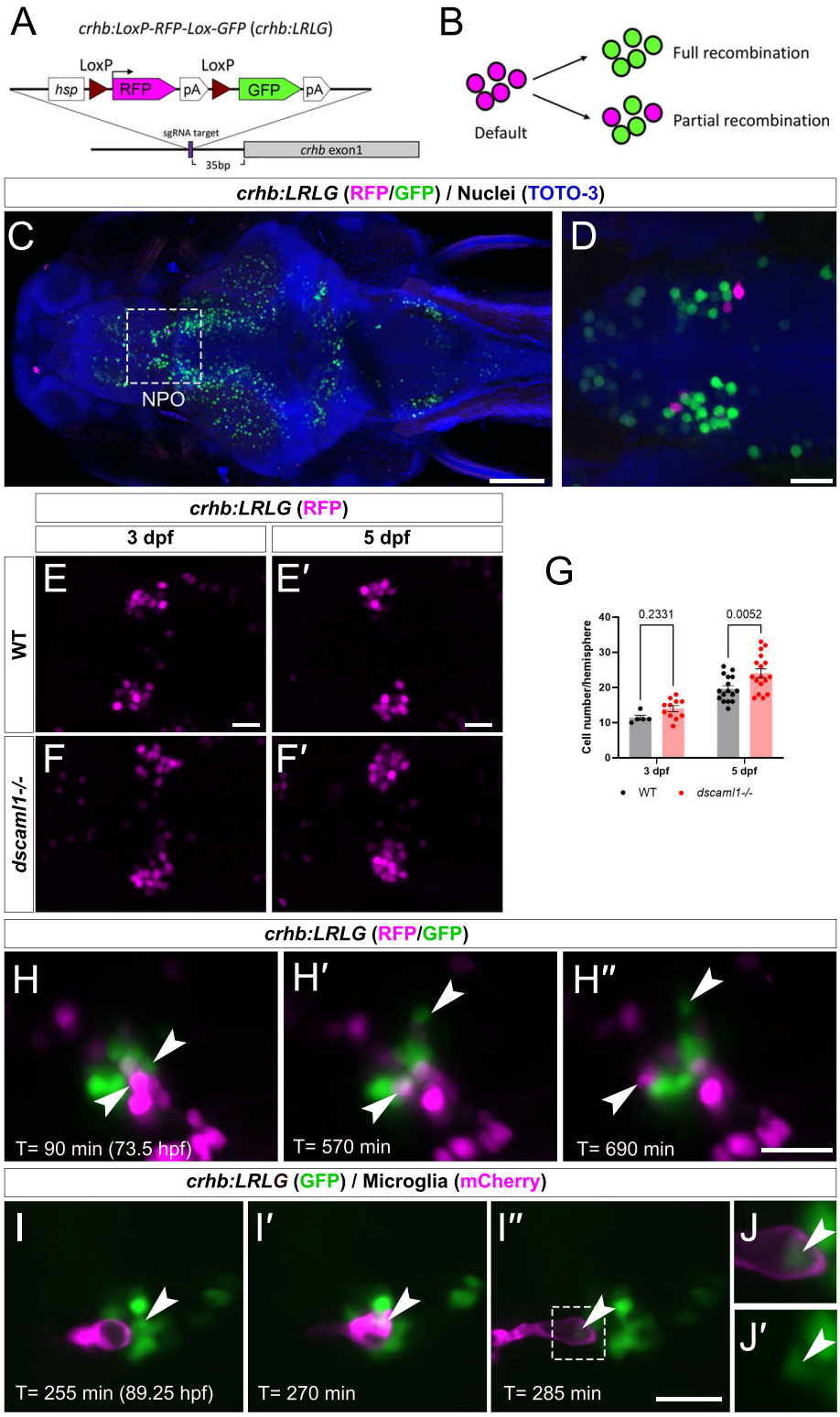
A
crhb:LoxP-RFP-Lox-GFP (crhb:LRLG)
LoxP
LoxP
hsp
RFP
pA
GFP
pA
sgRNA target
crhb exon1
35bp
B
Default
Full recombination
Partial recombination
crhb:LRLG (RFP/GFP) / Nuclei (TOTO-3)
C
NPO
D
crhb:LRLG (RFP)
3 dpf
5 dpf
WT
dscaml1-/-
E
E′
F
F′
G
0.2331
0.0052
Cell number/hemisphere
40
30
20
10
0
3 dpf
5 dpf
WT
dscaml1-/-
crhb:LRLG (RFP/GFP)
H
H′
H″
T= 90 min (73.5 hpf)
T= 570 min
T= 690 min
crhb:LRLG (GFP) / Microglia (mCherry)
I
I′
I″
J
J′
T= 255 min (89.25 hpf)
T= 270 min
T= 285 min

Figure 5

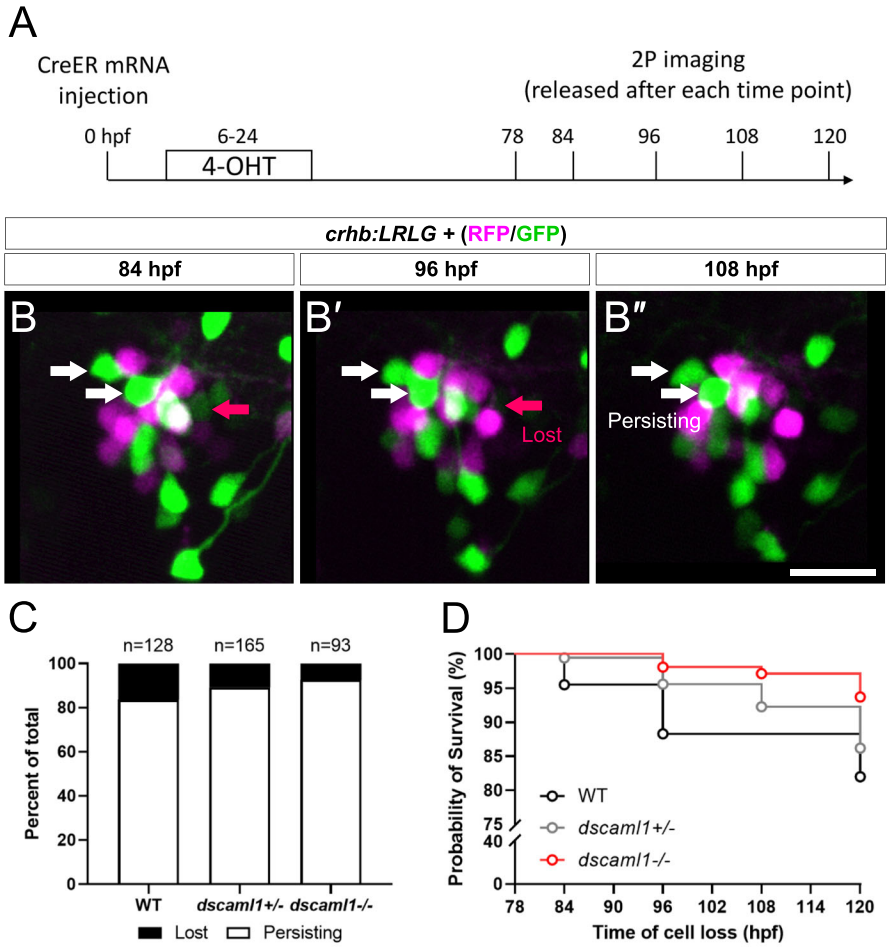
A
CreER mRNA injection
2P imaging (released after each time point)
0 hpf
6-24
4-OHT
78
84
96
108
120
crhb:LRLG + (RFP/GFP)
84 hpf
96 hpf
108 hpf
B
B′
B″
Lost
Persisting
C
n=128
n=165
n=93
Percent of total
WT
dscaml1+/-
dscaml1-/-
Lost
Persisting
D
Probability of Survival (%)
WT
dscaml1+/-
dscaml1-/-
Time of cell loss (hpf)

Figure 6

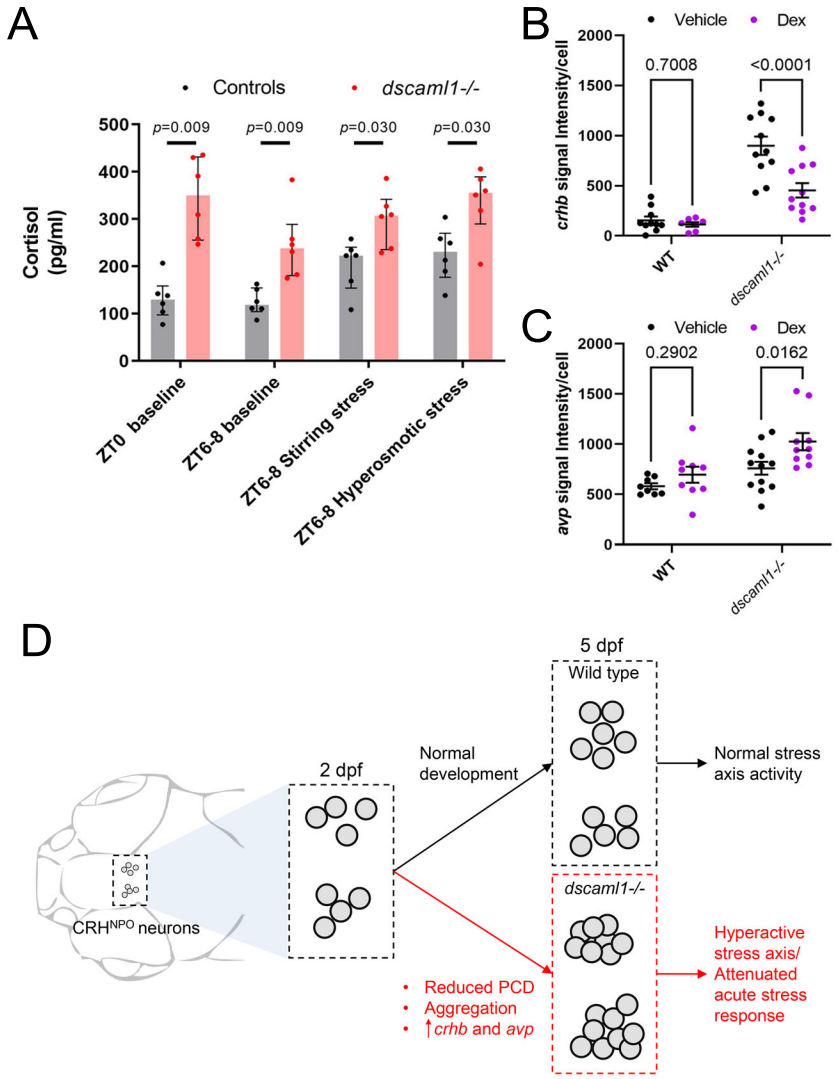
A
Controls
dscaml1-/-
Cortisol (pg/ml)
p=0.009
p=0.009
p=0.030
p=0.030
ZT0 baseline
ZT6-8 baseline
ZT6-8 Stirring stress
ZT6-8 Hyperosmotic stress
B
Vehicle
Dex
crhb signal Intensity/cell
0.7008
<0.0001
WT
dscaml1-/-
C
Vehicle
Dex
avp signal Intensity/cell
0.2902
0.0162
WT
dscaml1-/-
D
5 dpf
Wild type
2 dpf
Normal development
Normal stress axis activity
CRHNPO neurons
dscaml1-/-
Reduced PCD
Aggregation
↑crhb and avp
Hyperactive stress axis/ Attenuated acute stress response

Figure 7

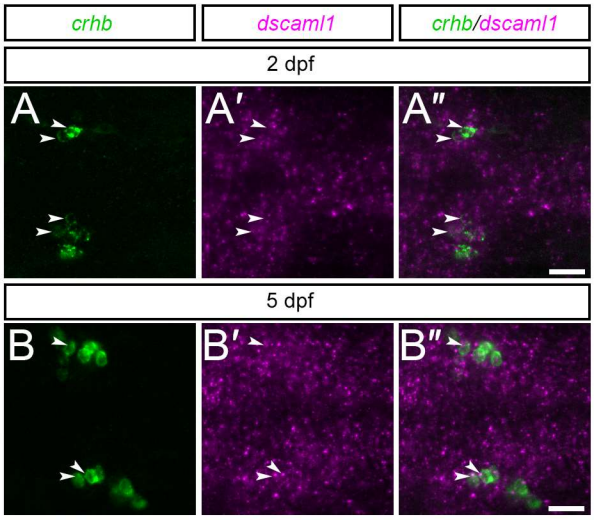

Supp. Fig. 1

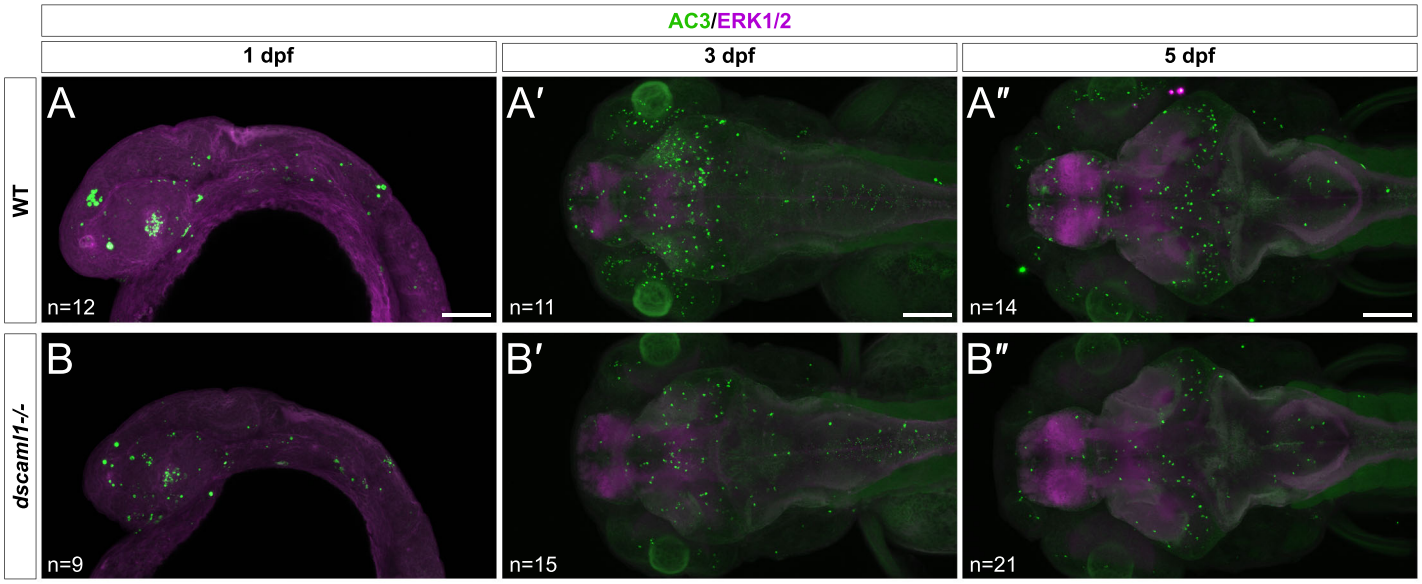
AC3/ERK1/2
1 dpf
3 dpf
5 dpf
WT
dscaml1-/-
A
A′
A″
B
B′
B″
n=12
n=11
n=14
n=9
n=15
n=21

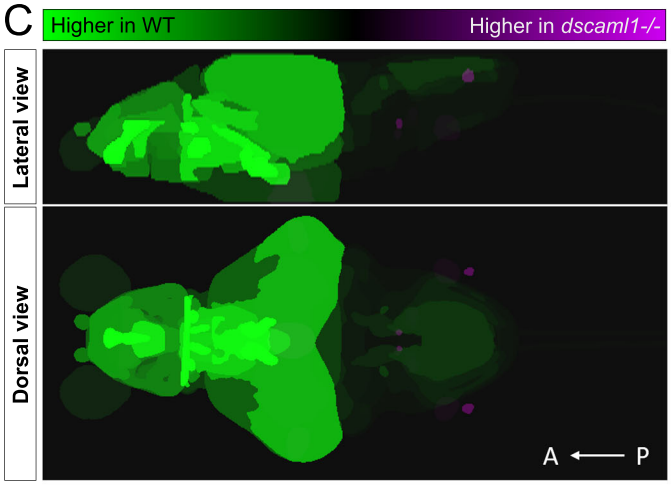
C
Higher in WT
Higher in dscaml1-/-
Lateral view
Dorsal view
A
P

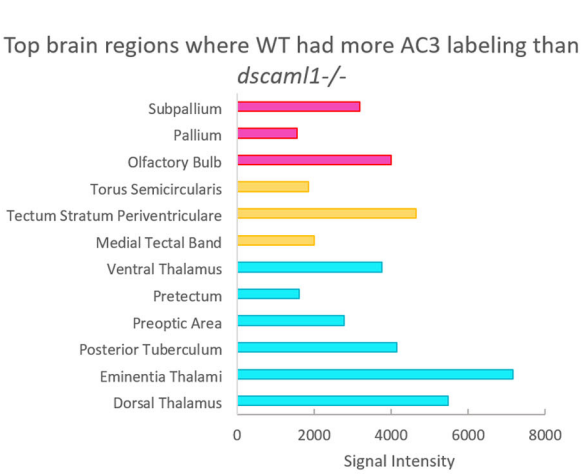
D
Top brain regions where WT had more AC3 labeling than dscaml1-/-
Subpallium
Pallium
Olfactory Bulb
Torus Semicircularis
Tectum Stratum Periventriculare
Medial Tectal Band
Ventral Thalamus
Pretectum
Preoptic Area
Posterior Tuberculum
Eminentia Thalami
Dorsal Thalamus
0
2000
4000
6000
8000
Signal Intensity

Supp. Fig. 2

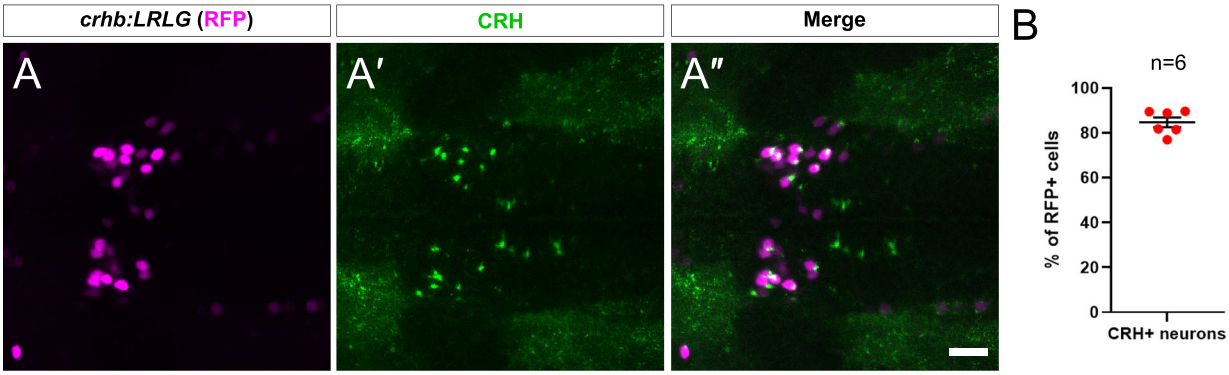
crhb:LRLG (RFP)
CRH
Merge
A
A′
A″
B
n=6
% of RFP+ cells
100
80
60
40
20
0
CRH+ neurons

Supp. Fig. 3